Received: Added at production | Revised: Added at production | Accepted: Added at production

DOI: xxx/xxxx

ARTICLE TYPE

Digital Twin Data Modelling by Randomized Orthogonal Decomposition and Deep Learning

Diana Alina Bistrian*[1] | Omer San[2] | Ionel Michael Navon[3]

[1]Department of Electrical Engineering and Industrial Informatics, University Politehnica Timisoara, Romania
[2]School of Mechanical & Aerospace Engineering, Oklahoma State University, USA
[3]Department of Scientific Computing, Florida State University, USA

Correspondence
*Diana A. Bistrian, Email: diana.bistrian@upt.ro

Summary

A digital twin is a surrogate model that has the main feature to mirror the original process behavior. Associating the dynamical process with a *digital twin model of reduced complexity* has the significant advantage to map the dynamics with high accuracy and reduced costs in CPU time and hardware to timescales over which that suffers significantly changes and so it is difficult to explore. This paper introduces a new framework for creating efficient digital twin models of fluid flows. We introduce a novel algorithm that combines the advantages of Krylov based dynamic mode decomposition with proper orthogonal decomposition and outperforms the selection of the most influential modes. We prove that randomized orthogonal decomposition algorithm provides several advantages over SVD empirical orthogonal decomposition methods and mitigates the projection error formulating a multiobjective optimization problem. We involve the state-of-the-art artificial intelligence Deep Learning (DL) to perform a real-time adaptive calibration of the digital twin model, with increasing fidelity. The output is a high-fidelity DIGITAL TWIN DATA MODEL of the fluid flow dynamics, with the advantage of a reduced complexity. The new modelling tools are investigated in the numerical simulation of three wave phenomena with increasing complexity. We show that the outputs are consistent with the original source data. We perform a thorough assessment of the performance of the new digital twin data models, in terms of numerical accuracy and computational efficiency, including a time simulation response feature study.

KEYWORDS:
digital twin data model, randomized orthogonal decomposition, Hopf-Cole-Transformation, deep learning

1 | INTRODUCTION

Due to increasing computational power and sophisticated experimental equipment, researchers have to interpret large datasets of numerical or experimental origin, therefore data science has become a paramount field of research. Researchers' interests were directed in recent years to identification of a reliable approximation of the complex behaviour of raw data by models of low complexity, i.e. reduced order models (ROM). This is possible given the fact that these complex systems exhibit low-dimensional patterns dominated by a number of underlying coherent structures [1], having different contribution or weights in the reconstitution of the data.

Any complex data system often consists of a superposition of such coherent structures, whose development is responsible for the bulk mass, momentum and energy transfer. Once the most influential coherent structures are identified, it is assumed that these contain the essential behavior of the system and the ROM is constructed by overlapping them. The patterns having insignificant contribution are ignored.

Depending on the mathematical approach with which they were built, ROM models have various computational qualities. The construction of high fidelity ROM models has become both science and art.

A digital twin is a surrogate model that has the main feature to mirror the original process behavior[2]. Associating the dynamical process with a *digital twin model of reduced complexity* has the significant advantage to map the dynamics with high accuracy and reduced costs in CPU time and hardware to timescales over which that suffers significantly changes and so it is difficult to explore.

This paper introduces a new framework for creating high fidelity reduced order models in fluid dynamics, having by definition the smallest error and the highest correlation in relation to the original data, models that we are calling *digital twin data models (DTM)* .

1.1 | Powerful Tools on ROM and Previous Work

Among several model order reduction techniques that performs well with non-intrusive data, Proper Orthogonal Decomposition (POD) and Dynamic Mode Decomposition (DMD) are widely applied to create surrogate models of dynamics of complex systems in different applications.

The well known method of POD has been illustrated on a variety of examples ranging from turbulent flows (Wang et al.[3], Xiao et al.[4]), convection-dominated flows (Gunzburger et al.[5]), fluid mechanics (Luchtenburg and Rowley[6], Liberge and Hamdouni[7], Xiao et al.[8]), oceanography (San et al.[9,10], Dumon et al.[11], Osth et al.[12]) to engineering applications (Buljak and Maier[13], Brunton and Kutz[14]) or aerodynamics (Xiao et al.[15], Li et al.[16]). POD approach has been incorporated for reduced order modeling purposes by many practitioners, for exemplification see Kaiser et al.[17], Wang et al.[18], Stefanescu et al.[19], Dimitriu et al.[20]. POD proved to be an effective technique also in inverse problems (Winton et al.[21], Chen et al.[22,23] and Cao et al.[24,25]) and also in association with data assimilation techniques (Xiao et al.[26]) and control (Sierra et al.[27], Dawson and Brunton[28]). Recently POD was involved in harnessing the power of Machine Learning tools, especially artificial neural networks (ANNs) for reduced order modeling in the inquiry work of Xiao et al.[29], San et al.[30], Kaptanoglu et al.[31], Owens and Kutz[32], Cheng et al.[33].

The intrusive model order reduction is usually derived by combining the POD and the Galerkin projection methods[34,10]. This approach suffers from efficiency issues and it lacks stability because the Galerkin projection is mathematically performed by laborious calculation and requires stabilization techniques in the process of numerical implementation, as it was argued in[35,36,37,38,39].

Koopman Mode Decomposition (KMD)[40] introduced by the French-born American mathematician B. O. Koopman, provides a theoretical background for modal decomposition, global modes analysis and hydrodynamic stability in problems describing oscillating phenomena. Once it was proved by Mezić[41,42] that normal modes of linear oscillations (or *shape modes*) have their natural analogs Koopman modes in the context of nonlinear dynamics, the Koopman theory was intensively applied for the purposes of reduced order modelling[43,44,45,46]. Schmid and Sesterhenn[47] were the first to introduce a numerical algorithm to compute this type of modal decomposition that was called Dynamic Mode Decomposition (DMD). In a bold manner, Rowley and his coworkers[48] proved that the linearity assumption of the Koopman operator is not necessary in order to derive the DMD. Schmid[49] explored the similarities between POD and DMD and introduced a more well conditioned DMD algorithm. Recently, Mezić[50], provides a characterization of Koopman modes in Banach spaces using Generalized Laplace Analysis.

Multiple applications of DMD originated in the fluid dynamics community[51,52,53,54,55] and recently this technique emerged into the niche fields like neuroscience (Brunton et al.[56]), machine learning (Kutz et al.[57], Percic et al.[58], Pant et al.[59]), epidemiology (Bistrian et al.[60,61], Zheng et al.[62], Kim et al.[63]).

A considerable amount of work has focused on understanding and improving the method of dynamic mode decomposition and several variants of DMD have been released: optimized DMD (Chen et al.[44]), exact DMD (Tu et al.[64]), sparsity promoting DMD (Jovanovic et al.[65]), multi-resolution DMD (Kutz et al.[66]), extended DMD (Williams et al.[67]), recursive dynamic mode decomposition (Noack et al.[68]), DMD with control (Proctor et al.[69]), randomized low-rank DMD (Erichson and Donovan[70]), compressed DMD (Erichson et al.[71]), adaptive randomized DMD (Bistrian and Navon[72]), dynamic mode decomposition with core sketch (Ahmed et al.[73]), bilinear dynamic mode decomposition (Goldschmidt et al.[74]), higher order dynamic mode decomposition (Le Clainche and Vega[75]).

A comparison of DMD vs. POD in reduced order modelling was illustrated in our previous paper[34], for the study of shallow water equations model. Although spatial basis functions for DMD and POD respectively, offer an insight of the coherent structures in the flow field, there are several major differences between these two ROM techniques. POD computes a set of orthonormal basis vectors associated with the most influential modes by which the given data is characterized, which are energetically ranked. The most energetic POD modes are selected to generate the ROM. The applicability of POD to complex systems is limited mainly due to errors associated with the truncation of POD modes[22,76,77].

Unlike POD, each DMD shape mode is associated with a pulsation, a growth rate and each mode has a single distinct frequency. Selection of Koopman modes used for the flow reconstruction constitutes the source of many discussions among modal decomposition practitioners. It was reported that neither the selection of the modes based on their amplitude, nor the selection based on the frequency are certain to lead to the finding of the dominant modes[78,79].

We have done in our previous papers an extensive research on several procedures for selecting the most influential modes in dynamic mode decomposition and we'll briefly mention them. In[34] we proposed a framework for modal decomposition of $2D$ flows, when numerical data are captured with large time steps. We arranged the modes in descending order of their energy weighted by the inverse of the Strouhal number. The modes that contribute weakly to the data sequence were eliminated based on the conservation of quadratic integral invariants[80] by the reduced order flow. In[81] we proposed a new framework for dynamic mode decomposition based on the reduced Schmid operator. We investigated a variant of DMD algorithm and we explored the selection of the modes based on sorting them in decreasing order of their amplitudes. This procedure works well for models without modes that are very rapidly damped, having very high amplitudes. Therefore the selection of modes based on their amplitude is effective only in certain situations. In[82] we focused on the effects of modes selection in dynamic mode decomposition. We proposed a dynamic filtering criterion for which the amplitude of any mode is weighted by its growth rate, resulting in identification of dynamically relevant flow features of time-resolved numerical data. The major disadvantage of this method lies in the fact that DMD does not produce orthogonal modes, therefore it will require a relatively large number of modes. Although the reported results were satisfactory, defining a DMD modes'selection criterion requires additional attention in the offline stage of the algorithm and increases the CPU time.

To overcome this inconvenient of classic DMD, we have introduced in[72] the method of Adaptive Randomized Dynamic Mode Decomposition (ARDMD) with application to fluid dynamics and we proved its efficiency on several applications[83]. Still, because this algorithm does not produce orthogonal modes either, there are difficulties in calibrating the model when simulating it in time.

1.2 | Significance and Novelty of the Present Research

To circumvent the aforementioned shortcomings of existing methods, in this paper we aim to achieve two major objectives:
1. To represent with highest precision the original data through the digital twin data model (DTM), having as few terms as possible;
2. To produce shape modes that are qualitatively superior in comparison with other techniques.

To achieve these goals, we introduce several key innovations.

We introduce a novel algorithm that produces shape modes that are orthonormal to each other. We prove that the shape modes maximize their projection on the data space in comparison with SVD empirical decomposition technique, thus we need a smaller number of terms in the model. We prove that randomized orthogonal decomposition algorithm provides several advantages over SVD empirical orthogonal decomposition and mitigates the projection error formulating a multiobjective optimization problem.

We avoid a computationally expensive algorithm and we reduce the problem dimension by using a randomized singular value decomposition (RSVD) technique. As we have previously demonstrated in[72,82,83], including randomization in the algorithm has the major benefit of not requiring additional criteria to select the shape modes, as it is done in case of DMD and POD.

We ensure the best correlation between the digital twin data model (DTM) and the original raw data by involving the state-of-the-art artificial intelligence Deep Learning (DL) to perform a real-time adaptive calibration of the model.

We shall refer to this procedure as **Randomized Orthogonal Decomposition (ROD)**. We involve the state-of-the-art artificial intelligence Deep Learning (DL) to perform a real-time adaptive calibration of the model, toward an increasing fidelity model. The output is a high-fidelity DIGITAL TWIN DATA MODEL of the fluid flow dynamics, with the advantage of a reduced complexity.

To the best of our knowledge, in the present research we perform the first study of the quality of the shape modes and we demonstrate that the ROD shape modes maximize their projection on the data space.

The new algorithm is investigated in the numerical simulation of the viscous Burgers equation model with three different initial conditions, leading to wave phenomena of increasing complexity. We show that the outputs are consistent with the original source data. We perform a thorough assessment of the performance of the new digital twin data models produced by ROD with DL, in terms of numerical accuracy and computational efficiency, including a time simulation response study.

The remainder of the article is organized as follows. In Section 2 the test problem consisting of the nonlinear viscous Burgers equation model is presented. In Section 3 we introduce mathematical considerations regarding the SVD empirical orthogonal representation and we provide the description of the novel randomized orthogonal decomposition algorithm (ROD). We introduce a novel theorem that states that the ROD modes are qualitatively superior to SVD empirical orthogonal modes and we provide the proof of the theorem. In section 4 we describe the technique of fast digital twin data model identification using deep learning. Section 5 presents the numerical results together with a computational efficiency study. Summary and conclusions are drawn in the final section.

2 | MATHEMATICAL MODELS

2.1 | Mathematical Model Equations

We consider the viscid Burgers equation model of the form:

$$\begin{cases} \frac{\partial}{\partial t}u(x,t) + \frac{\partial}{\partial x}\left(\frac{u(x,t)^2}{2}\right) = \nu\frac{\partial^2}{\partial x^2}u(x,t), \quad t>0, \quad \nu>0, \\ u(x,0) = u_0(x), \quad x\in\mathbb{R}, \end{cases} \tag{1}$$

where $u(x,t)$ is the unknown function of time t, ν is the viscosity parameter.

We will consider three experiments, respectively having the initial condition of the form:

$$Experiment\ 1: \quad u_0(x) = -\sin(\pi x), \tag{2}$$

$$Experiment\ 2: \quad u_0(x) = \begin{cases} u_L, & x\le 0 \\ u_R, & x>0 \end{cases}, \tag{3}$$

$$Experiment\ 3: \quad u_0(x) = -\cos(1.5\pi x)^2. \tag{4}$$

The homogeneous Dirichlet boundary conditions of the form

$$u(0,t) = u(L,t) = 0 \tag{5}$$

are applied for all three examples.

The Cole-Hopf transformation, introduced by Cole (1951) and Hopf (1950) independently, transforms the equation (1) into the heat equation and therefore it can be solved to obtain the exact solution. We introduce the Cole-Hopf transformation in the next section.

2.2 | The Exact Solution: The Cole-Hopf Transformation

The Cole-Hopf transformation is defined by

$$u = -2\nu\frac{1}{\varphi}\frac{\partial\varphi}{\partial x}. \tag{6}$$

Through an analytical handling we find that

$$\frac{\partial u}{\partial t} = \frac{2\nu}{\varphi^2}\left(\frac{\partial\varphi}{\partial t}\frac{\partial\varphi}{\partial x} - \varphi\frac{\partial^2\varphi}{\partial x\partial t}\right), \quad u\frac{\partial u}{\partial x} = \frac{4\nu^2}{\varphi^3}\frac{\partial\varphi}{\partial x}\left(\varphi\frac{\partial^2\varphi}{\partial x^2} - \frac{\partial\varphi}{\partial x}\frac{\partial\varphi}{\partial x}\right), \tag{7}$$

$$\nu\frac{\partial^2 u}{\partial x^2} = -\frac{2\nu^2}{\varphi^3}\left(2\left(\frac{\partial\varphi}{\partial x}\right)^3 - 3\varphi\frac{\partial^2\varphi}{\partial x^2}\frac{\partial\varphi}{\partial x} + \varphi^2\frac{\partial^3\varphi}{\partial x^3}\right). \tag{8}$$

Substituting these expressions into (1) it follows that

$$\frac{\partial\varphi}{\partial x}\left(\frac{\partial\varphi}{\partial t} - \nu\frac{\partial^2\varphi}{\partial x^2}\right) = \varphi\left(\frac{\partial^2\varphi}{\partial x\partial t} - \nu\frac{\partial^3\varphi}{\partial x^3}\right) = \varphi\frac{\partial}{\partial x}\left(\frac{\partial\varphi}{\partial t} - \nu\frac{\partial^2\varphi}{\partial x^2}\right). \tag{9}$$

Relation (9) indicates that if φ solves the heat equation, then $u(x,t)$ given by the Cole-Hopf transformation (6) solves the viscid Burgers equation (1). Thus we have reduced the viscid Burgers equation (1) to the following one

$$\begin{cases} \frac{\partial \varphi}{\partial t} - \nu \frac{\partial^2 \varphi}{\partial x^2} = 0, \quad x \in R, t > 0, \nu > 0, \\ \varphi(x,0) = \varphi_0(x) = e^{-\int_0^x \frac{u_0(\xi)}{2\nu} d\xi}, x \in \mathbb{R}. \end{cases} \tag{10}$$

Taking the Fourier transform with respect to x for both heat equation and the initial condition (10) we obtain the analytic solution

$$\varphi(x,t) = \frac{1}{2\sqrt{\pi \nu t}} \int_{-\infty}^{\infty} \varphi_0(\xi) e^{-\frac{(x-\xi)^2}{4\nu t}} d\xi. \tag{11}$$

From the Cole-Hopf transformation (6) we obtain the analytic solution to the problem (1) in the following form

$$u(x,t) = \frac{\int_{-\infty}^{\infty} \frac{x-\xi}{t} \varphi_0(\xi) e^{-\frac{(x-\xi)^2}{4\nu t}} d\xi}{\int_{-\infty}^{\infty} \varphi_0(\xi) e^{-\frac{(x-\xi)^2}{4\nu t}} d\xi}. \tag{12}$$

2.3 | Gauss-Hermite Quadrature

In order to calculate the exact solution (12) with the initial conditions of the three test cases (2)-(4), we asses the technique of Gauss-Hermite Quadrature [84]. Gauss–Hermite quadrature approximates the value of integrals of the following kind:

$$\int_{-\infty}^{\infty} f(z) e^{-z^2} dz \approx \sum_{i=1}^{n} w_i f(x_i), \tag{13}$$

where n represents the number of sample points used, x_i are the roots of the Hermite polynomial $H_n(x)$ and the associated weights w_i are given by

$$w_i = \frac{2^{n-1} n! \sqrt{\pi}}{n^2 \left(H_{n-1}(x_i)\right)^2}, \quad i = 1, ..., n. \tag{14}$$

In the case of Experiment 1, the initial condition is given by Eq.(2) and we have

$$\varphi_0(x) = e^{-\frac{1}{2\nu}\int_0^x u_0(\xi) d\xi} = e^{-\frac{1}{2\nu}\int_0^x -\sin(\pi\xi) d\xi} = e^{\frac{1}{2\nu\pi}} \cdot e^{-\frac{\cos(\pi x)}{2\nu\pi}}. \tag{15}$$

We cast the exact solution (12) in form

$$u(x,t) = \frac{\int_{-\infty}^{\infty} \frac{x-\xi}{t} e^{-\frac{\cos(\pi\xi)}{2\nu\pi}} \cdot e^{-\left(\frac{x-\xi}{\sqrt{4\nu t}}\right)^2} d\xi}{\int_{-\infty}^{\infty} e^{-\frac{\cos(\pi\xi)}{2\nu\pi}} \cdot e^{-\left(\frac{x-\xi}{\sqrt{4\nu t}}\right)^2} d\xi}. \tag{16}$$

We introduce the variable change

$$z = \frac{x-\xi}{\sqrt{4\nu t}}, \tag{17}$$

so the exact solution to the Burgers equation model (1) with the initial condition (2) is

$$u(x,t) = \frac{\int_{-\infty}^{\infty} 4\nu z \, e^{-\frac{1}{2\nu\pi}\cos\left[\pi\left(x - z\sqrt{4\nu t}\right)\right]} e^{-z^2} dz}{\int_{-\infty}^{\infty} \sqrt{4\nu t} \, e^{-\frac{1}{2\nu\pi}\cos\left[\pi\left(x - z\sqrt{4\nu t}\right)\right]} e^{-z^2} dz}. \tag{18}$$

In the similar manner, with the help of variable change (17), we obtain the exact solution for the next two experiments, as follows.

In the case of Experiment 2 the exact solution to the Burgers equation model (1) with the initial condition (3) is:

$$u(x,t) = \frac{\int_{-\infty}^{\infty} 4\nu z \, e^{-\frac{u_R}{2\nu}\left(x - z\sqrt{4\nu t}\right)} e^{-z^2} dz}{\int_{-\infty}^{\infty} \sqrt{4\nu t} \, e^{-\frac{u_R}{2\nu}\left(x - z\sqrt{4\nu t}\right)} e^{-z^2} dz}. \tag{19}$$

In the case of Experiment 3 the exact solution to the Burgers equation model (1) with the initial condition (4) is:

$$u(x,t)=\frac{\int_{-\infty}^{\infty}4\nu z\; e^{\frac{1}{4\nu}\left(\frac{1}{3\pi}\sin\left(3\pi(x-z\sqrt{4\nu t})\right)+x-z\sqrt{4\nu t}\right)}e^{-z^2}dz}{\int_{-\infty}^{\infty}\sqrt{4\nu t}\; e^{\frac{1}{4\nu}\left(\frac{1}{3\pi}\sin\left(3\pi(x-z\sqrt{4\nu t})\right)+x-z\sqrt{4\nu t}\right)}e^{-z^2}dz}. \tag{20}$$

In order to obtain the exact solutions in the three test cases, we calculate both the numerator and the denominator with the help of the Gauss-Hermite quadrature (13) with $n = 100$.

3 | A NOVEL RANDOMIZED ORTHOGONAL DECOMPOSITION ALGORITHM FOR DIGITAL TWIN DATA MODELLING

In this section we provide a description of the numerical method introduced in this paper to create the digital twin data models in the investigation of the Burgers equation models.

3.1 | Mathematical Considerations

Suppose that $D = [0, L] \subset \mathbb{R}$ represents the computational domain, we consider the space $L^2(D)$ of square integrable functions on D

$$L^2(D)=\left\{\phi\,:\,D\to\mathbb{R}\;\middle|\;\int_D|\phi|^2dx<\infty\right\} \tag{21}$$

be a Hilbert space endowed with the inner product

$$\left\langle\phi_i(x),\phi_j(x)\right\rangle_{L^2(D)}=\int_D\phi_i(x)\,\phi_j(x)\;dx\quad for\;\phi_i,\phi_j\in L^2(D) \tag{22}$$

and the induced norm $\|\phi\|_{L^2(D)}=\sqrt{\langle\phi,\phi\rangle_{L^2(D)}}$ for $\phi\in L^2(D)$.

We proceed by collecting data $u_i(x,t)=u\left(x,t_i,\right),\;t_i=i\Delta t,\;i=0,...,N_t$, representing the data measurements at the constant sampling time Δt, x representing the Cartesian spatial coordinate. Let the two integer parameters N_t and N_x having the following meanings:

$N_t + 1 = 300 + 1$ total number of snapshots taken in time,

$N_x = 101$ number of spatial measurements per time snapshot.

We form a data matrix whose columns represent the individual data samples, called *the snapshot matrix*

$$V=\left[u_0\;u_1\;...\;u_{N_t}\right]\in\mathbb{R}^{N_x\times(N_t+1)}. \tag{23}$$

Each column $u_i\in\mathbb{R}^{N_x}$ is a vector with N_x components, representing the spatial measurements corresponding to the $N_t + 1$ time instances.

We concentrate on approximating the exact solution (12) to the Burgers problem (1)-(5) as a finite sum of products between a time dependent part and steady-state component of the form

$$u(x,t)\approx\sum_{i=1}^{r}a_i(t)\,\phi_i(x), \tag{24}$$

expecting that this approximation becomes exact as $r\to+\infty$.

Proposition 1. (Empirical Orthogonal Decomposition)

Let

$$V=\left[u_0\;u_1\;...\;u_{N_t}\right]\in\mathbb{R}^{N_x\times(N_t+1)}$$

be a real-valued data matrix of rank $r\le\min\left(N_x,N_t+1\right)$, whose columns $u_j\in\mathbb{R}^{N_x}$, $j = 1, ..., N_t + 1$ are data snapshots. The Singular Value Decomposition (SVD) yields the factorization

$$V=\Psi\Sigma\Phi^T \tag{25}$$

of the matrix V, where $\Psi = \left[\psi_1, ..., \psi_{N_x}\right] \in \mathbb{R}^{N_x \times N_x}$ and $\Phi = \left[\varphi_1, ..., \varphi_{N_t+1}\right] \in \mathbb{R}^{(N_t+1)\times(N_t+1)}$ are orthogonal matrices,

$$\Sigma = \begin{pmatrix} D & 0 \\ 0 & 0 \end{pmatrix} \in \mathbb{R}^{N_x \times (N_t+1)},$$

with $D = diag\left(\sigma_1, ..., \sigma_r\right) \in \mathbb{R}^{r\times r}$ and $\sigma_1 \geq \sigma_2 \geq ... \geq \sigma_r > 0$. Then $\left\{\psi_i\right\}_{i=1}^r$ and $\left\{\varphi_i\right\}_{i=1}^r$ represent the eigenvectors of VV^T and V^TV, respectively, with eigenvalues $\lambda_i = \sigma_i^2 > 0$ for $i = 1, ..., r$, due to the relations

$$V\varphi_i = \sigma_i\psi_i \quad and \quad V^T\psi_i = \sigma_i\varphi_i \quad for\ i = 1, ..., r.$$

It follows that

$$V = \sum_{i=1}^{r} \sigma_i\psi_i\varphi_i^T. \tag{26}$$

From (26) we deduce that

$$\begin{aligned} u_j &= \sum_{i=1}^{r} \left[D\Phi^T\right]_{ij}\psi_i = \sum_{i=1}^{r} \left[\overbrace{\Psi^T\Psi}^{=I\in\mathbb{R}^{r\times r}} D\Phi^T\right]_{ij}\psi_i \\ &= \sum_{i=1}^{r} \left[\Psi^TV\right]_{ij}\psi_i = \sum_{i=1}^{r} \left\langle u_j, \psi_i\right\rangle_{L^2(D)}\psi_i. \end{aligned} \tag{27}$$

The representation (27) is called the Fourier representation of u_j or empirical orthogonal decomposition. This is the foundation for more advanced decomposition algorithms, like POD and DMD.

In the case of linearly-independent snapshots, the empirical orthogonal decomposition involves a number of terms equal to $r = \min\left(N_x, N_t + 1\right)$, which can be a large number. By convention, let suppose that $\mathrm{r} = \min\left(N_x, N_t + 1\right) = N_x$. We denote by *full empirical orthogonal representation*, the following relation

$$u^{Fourier}(x,t) = \sum_{i=1}^{N_x} a_i(t)\,\psi_i(x), \quad a_i(t) = \langle u, \psi_i\rangle_{L^2(D)}. \tag{28}$$

In practice, the full empirical orthogonal representation is not convenient do to the large number of unknown functions. We introduce in the following a novel algorithm to produce the representation (24).

We seek an orthonormal base of functions, i.e.

$$\Phi = \left\{\phi_1, \phi_2, ...\right\}, \quad \left\langle \phi_i(x), \phi_j(x)\right\rangle_{L^2(D)} = \delta_{ij}, \quad \|\phi\|_{L^2(D)} = 1, \tag{29}$$

where δ_{ij} is the Kronecker delta symbol

$$\delta_{ij} = \begin{cases} 1 & if \quad i = j \\ 0 & if \quad i \neq j \end{cases} \tag{30}$$

consisting of a minimum number of functions $\phi_i(x)$, such that the approximation of $u(x,t)$ through this base is *as good as possible*, i.e. we aim to create a *digital twin model* for data snapshots, of reduced complexity.

Technically, the digital twin data model (DTM) at every time step $\left\{\mathrm{t}_1,...,\mathrm{t}_{N_t}\right\}$ is written according to the following relation:

$$u^{DTM}\left(x, t_i\right) = \sum_{j=1}^{N_{DTM}} \underbrace{a_j\left(t_i\right)}_{Modal\ amplitudes} \overbrace{\phi_j(x)}^{Leading\ shape\ modes}, \ t_i \in \left\{\mathrm{t}_1, ..., \mathrm{t}_{N_t}\right\}, \tag{31}$$

where $\phi_j \in \mathbb{C}$ represent the Φ base functions which we call *the leading shape modes*, $N_{DTM} \ll \min\left(N_x, N_t + 1\right)$ represents the number of terms in the representation (31) which we impose to be minimal and $a_j\left(t_i\right)$ represent the modal growing amplitudes.

Our objective is to represent with highest precision the original data through the digital twin data model (31) having as few terms as possible. To achieve this goal, we introduce several major innovative features in our algorithm:

- We produce shape modes that are orthonormal to each other, which means that we will need a small number of terms in (31);
- We avoid a computationally expensive algorithm and we reduce the problem dimension by using a randomized singular value decomposition (RSVD) technique. The efficiency of this technique was previously demonstrated in [72,82,83,85,86].

Including randomization in the algorithm has the major benefit of not requiring additional criteria to select the shape modes, as it is done in case of techniques like dynamic mode decomposition (DMD) or proper orthogonal decomposition (POD). Our algorithm that includes the RSVD finds the optimal reduced order subspace that contains the leading shape modes base Φ.

- We ensure the best correlation between the digital twin data model (31) and the exact solution (12) by searching for the leading shape modes that approximate the data sequence with smallest error.

Determination of the optimal decomposition (31) then amounts to finding the solution to the following multiobjective constrained optimization problem:

$$\begin{aligned}
&\min_{\phi_j, a_j, N_{DTM}} \sum_{i=1}^{N_t} \int_D \left\| u\left(x,t_i\right) - \sum_{j=1}^{N_{DTM}} a_j\left(t_i\right)\phi_j\left(x\right) \right\|^2_{L^2(D)} dx, \\
&\min_{\phi_j, a_j, N_{DTM}} \sum_{i=1}^{N_t} \int_D \frac{-\left\| u(x,t_i) \sum_{j=1}^{N_{DTM}} a_j(t_i)\phi_j(x) \right\|^2_{L^2(D)}}{\left\| u(x,t_i)^H u(x,t_i) \right\|^2_{L^2(D)} \left\| \left(\sum_{j=1}^{N_{DTM}} a_j(t_i)\phi_j(x) \right)^H \sum_{j=1}^{N_{DTM}} a_j(t_i)\phi_j(x) \right\|^2_{L^2(D)}} dx, \\
&s.t. \quad \left\langle \phi_i, \phi_j \right\rangle_{L^2(D)} = \delta_{ij}, \quad \left\| \phi_i \right\|_{L^2(D)} = 1, \quad 1 \le i \le j \le N_{DTM}
\end{aligned} \tag{32}$$

where H denotes the conjugate transpose of the snapshot containing the data.

Mathematically, we are constructing the leading shape modes base $\left\{\phi_i\right\}_{i=1}^{N_{DTM}}$, which contains the smallest possible number of orthonormal vectors that maximize their projection on the data space.

Definition 1. (The Projection Operator)

Let

$$V_0 = \left[u_0 \; u_1 \; \ldots \; u_{N_t-1} \right] \equiv \left\{ u_i^0 \right\}_{i=0}^{N_t-1} \in \mathbb{R}^{N_x \times N_t}$$

be a real-valued data matrix, whose columns are data snapshots.

Let

$$\Phi = \left\{ \phi_1, \phi_2, ..., \phi_{N_{DTM}} \right\}$$

be a shape modes base.

We define the bounded projection operator $P_{V_0}\Phi$, that maps every shape mode $\left\{\phi_i\right\}_{i=1}^{N_{DTM}}$ onto its projection on the data vectors $\left\{u_i^0\right\}_{i=0}^{N_t-1}$ along the computational domain direction D:

$$P_{V_0}\Phi\left(\phi_i, u_j^0\right) \equiv P_{u_j^0}\phi_i = \left(\left\langle \phi_i, u_j^0 \right\rangle_{L^2(D)} / \left\langle u_j^0, u_j^0 \right\rangle_{L^2(D)} \right) u_j^0. \tag{33}$$

Proposition 2. (Randomized Singular Value Decomposition of rank k: k-RSVD)

Let

$$V_0 = \left[u_0 \; u_1 \; \ldots \; u_{N_t-1} \right] \in \mathbb{R}^{N_x \times N_t}$$

be a real-valued data matrix, whose columns are data snapshots. If we impose a target rank $k < \min\left(N_x, N_t\right)$, the Randomized Singular Value Decomposition of rank k (k-RSVD) produces k left singular vectors of V_0 and has the following steps:

1. Generate a Gaussian random test matrix M of size $N_t \times k$.
2. Compute a compressed sampling matrix by multiplication of data matrix with random matrix $Q = V_0 M$.
3. Project the data matrix to the smaller space $P = Q^H V_0$, where H denotes the conjugate transpose.
4. Produce the economy-size singular value decomposition of low-dimensional data matrix $[T, \Sigma, W] = svd\,(P)$.

   For the fact that the singular values (i.e., Σ) and the right singular vectors (i.e., W) of the matrix P are also the singular values and the right singular vectors of the original matrix V_0, we should preserve the singular values and the right singular vectors computed by the matrix P at this step.
5. Compute the right singular vectors $U = QT$, $U \in \mathbb{R}^{N_x \times k}$, $\Sigma \in \mathbb{R}^{k \times k}$, $W \in \mathbb{R}^{N_t \times k}$.

If we combine the matrix Q derived in the second step with the left singular vectors of P from step 4, we can get the left singular vectors of V_0 and Σ contains its singular values.

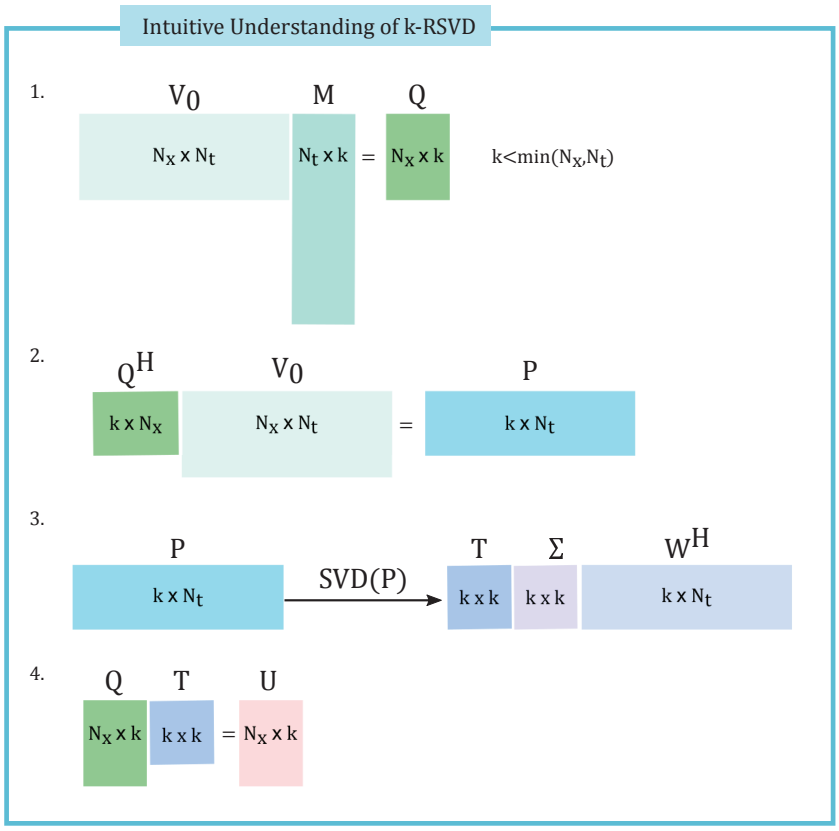

FIGURE 1 An intuitive understanding of k-RSVD producing the k left eigenvectors of snapshot matrix V_0.

An intuitive understanding of k-RSVD is illustrated in Figure 1.

Theorem 1. (Randomized Orthogonal Decomposition: ROD)

Let

$$\begin{aligned} V_0 &= \left[u_0 \ u_1 \ \ldots \ u_{N_t-1} \right] \equiv \left\{ u_i^0 \right\}_{i=0}^{N_t-1} \in \mathbb{R}^{N_x \times N_t}, \\ V_1 &= \left[u_1 \ u_2 \ \ldots \ u_{N_t} \right] \equiv \left\{ u_i^1 \right\}_{i=1}^{N_t} \in \mathbb{R}^{N_x \times N_t}, \end{aligned} \tag{34}$$

two time-shifted data matrices with rank r $\leq \min\left(N_x, N_t\right)$, whose columns are data snapshots. Then for $1 \leq N_{DTM} \leq r$, the optimization problem

$$\begin{aligned} &\max_{\phi_1,\ldots,\phi_{N_{DTM}}} \sum_{i=1}^{N_{DTM}} \sum_{j=1}^{N_t} \left\| P_{u_j^0} \phi_i \right\|_{L^2(D)}^2 \\ &s.t. \quad \left\langle \phi_i, \phi_j \right\rangle_{L^2(D)} = \delta_{ij}, \quad \left\| \phi_i \right\|_{L^2(D)} = 1, \quad 1 \leq i \leq j \leq N_{DTM} \end{aligned} \tag{35}$$

is being solved by the subspace $span\left\{\phi_1, \phi_2, ..., \phi_{N_{DTM}}\right\}$ spanned by the sequence of orthonormal functions

$$\left\{ \phi_i \right\}_{i=1}^{N_{DTM}} = \left\langle U, X_{.,i} \right\rangle_{L^2(D)} / \left\| \left\langle U, X_{.,i} \right\rangle \right\|_{L^2(D)} \tag{36}$$

where U represents the matrix of left singular vectors produced by Randomized Singular Value Decomposition of rank N_{DTM} of data matrix V_0 and X denotes the eigenvectors to the Koopman propagator operator $\mathcal{A}$, i.e.

$$\left\{ u_0, \ u_1 = \mathcal{A}u_0, \ u_2 = \mathcal{A}u_1 = \mathcal{A}^2 u_0, \ldots, \ u_{N_t} = \mathcal{A}u_{N_t-1} = \mathcal{A}^{N_t} u_0 \right\}. \tag{37}$$

Proof of Theorem 1. Following the Koopman decomposition assumption[40], we consider that a propagator operator $\mathcal{A}$ exists, that maps every column vector onto the next one, i.e.

$$\left\{ u_0, \ u_1 = \mathcal{A}u_0, \ u_2 = \mathcal{A}u_1 = \mathcal{A}^2 u_0, \ldots, \ u_{N_t} = \mathcal{A}u_{N_t-1} = \mathcal{A}^{N_t} u_0 \right\}. \tag{38}$$

For a sufficiently long sequence of the snapshots, we suppose that the last snapshot u_{N_t} can be written as a linear combination of previous N_t vectors, such that

$$u_{N_t} = c_0 u_0 + c_1 u_1 + ... + c_{N_t-1} u_{N_t-1} + \mathcal{R}, \tag{39}$$

in which $c_i \in \mathbb{R}$, i = 0,..., $N_t - 1$ and $\mathcal{R}$ is the residual vector. We assemble the following relations

$$\left\{u_1, u_2, ...u_{N_t}\right\} = \mathcal{A}\left\{u_0, u_1, ...u_{N_t-1}\right\} = \left\{u_1, u_2, ..., V_0 c\right\} + \mathcal{R}, \tag{40}$$

where $c = \begin{pmatrix} c_0 & c_1 & ... & c_{N_t-1} \end{pmatrix}^T$ is the unknown column vector.

Thus, we aim to solve the following eigenvalue problem

$$V_1 = \mathcal{A}V_0 = V_0 S + \mathcal{R}, \tag{41}$$

where S approximates the eigenvalues of $\mathcal{A}$ when $\|\mathcal{R}\|_2 \to 0$, which is equivalent to solve the minimization problem

$$\min_S \ \mathcal{R} = \left\|V_1 - V_0 S\right\|_2, \tag{42}$$

where $\|\cdot\|_2$ is the L_2-norm of $\mathbb{R}^{N_x}$.

Now, we aim to find the solution to the minimization problem (42).

Suppose that r $\leq \min\left(N_x, N_t\right)$. Then for $1 \leq N_{DTM} \leq r$, we identify the N_{DTM}-RSVD of V_0, that yields the factorization:

$$V_0 = U\Sigma W^H, \tag{43}$$

of the snapshot matrix V_0, where $U = \left[u_1, ..., u_{N_{DTM}}\right] \in \mathbb{R}^{N_x \times N_{DTM}}$ and $W = \left[w_1, ..., w_{N_{DTM}}\right] \in \mathbb{R}^{N_t \times N_{DTM}}$ are orthogonal matrices that contain the eigenvectors of $\mathrm{V_0 V_0}^H$ and $\mathrm{V_0}^H \mathrm{V_0}$, respectively, $\Sigma = diag\left(\sigma_1, ..., \sigma_{N_{DTM}}\right) \in \mathbb{R}^{N_{DTM} \times N_{DTM}}$ is a square diagonal matrix containing the singular values of V_0 and H means the conjugate transpose.

Relations $\mathcal{A}V_0 = V_1 = V_0 S + \mathcal{R}$, $\|\mathcal{R}\|_2 \to 0$ and $V_0 = U\Sigma W^H$ yield:

$$\begin{aligned} & \mathcal{A}U\Sigma W^H = V_1 = U\Sigma W^H S \\ \Rightarrow \quad & U^H \mathcal{A} U\Sigma W^H = U^H U\Sigma W^H S \\ \Rightarrow \quad & S = U^H \mathcal{A} U. \end{aligned}$$

From $\mathcal{A}U\Sigma W^H = V_1$ it follows that $\mathcal{A}U = V_1 W\Sigma^{-1}$ and hence $S = U^H\left(V_1 W\Sigma^{-1}\right)$.

The solution to the minimization problem (42) is the matrix operator

$$S = U^H\left(V_1 W\Sigma^{-1}\right). \tag{44}$$

A direct consequence of solving the minimization problem (42) is that decreasing the residual increases overall convergence and therefore the eigenvalues and the eigenvectors of S will converge toward the eigenvalues and the eigenvectors of the Koopman propagator operator $\mathcal{A}$.

Let $X \in \mathbb{R}^{N_{DTM} \times N_{DTM}}$, $\Lambda \in \mathbb{R}^{N_{DTM} \times N_{DTM}}$ be the eigenvectors, respectively the eigenvalues of the data propagator matrix S, as solution to the eigenvalue problem:

$$SX = X\Lambda. \tag{45}$$

Then, we define the subspace $\Phi = span\left\{\phi_1, \phi_2, ..., \phi_{N_{DTM}}\right\}$ spanned by the sequence of functions

$$\left\{\phi_i\right\}_{i=1}^{N_{DTM}} = \left\langle U, X_{.,i}\right\rangle_{L^2(D)} \tag{46}$$

where U represents the matrix of left singular vectors produced by Randomized Singular Value Decomposition of rank N_{DTM} of data matrix V_0. It follows that

$$\left\langle \phi_i, \phi_j\right\rangle_{L^2(D)} = \delta_{ij}, \quad 1 \leq i \leq j \leq N_{DTM} \tag{47}$$

i.e., Φ forms an orthogonal base to the data space. For more robustness, we will construct an orthonormal base of the form given by Eq.(36).

In the next section, we will show numerically that the Φ base vectors maximize their projection on the data space and they represent the solution to the constrained optimization problem (32), therefore they produce the digital twin data model with the expression given by Eq.(31).

□

Corollary 1. The base vectors $\left\{\phi_i\right\}_{i=1}^{N_{DTM}}$ defined by Eq.(36), respectively their corresponding modal coefficients $\left\{a_i\right\}_{i=1}^{N_{DTM}} = \left\langle U, X_{.,i}\right\rangle_{L^2(D)}$, solve the multiobjective constrained minimization problem (32).

Corollary 2. If

$$\left\| P_{V_0}\Phi \right\|^2_{L^2(D)} = \frac{1}{N_{DTM}} \sum_{i=1}^{N_{DTM}} \sum_{j=1}^{N_t} \left\| P_{u_j^0}\phi_i \right\|^2_{L^2(D)} \tag{48}$$

represents the mean squared sum of the norms of projections of shape modes $\left\{\phi_i\right\}_{i=1}^{N_{DTM}}$ produced by Randomized Orthogonal Decomposition on the data space V_0, and

$$\left\| P_{V_0}\Psi \right\|^2_{L^2(D)} = \frac{1}{N_x} \sum_{i=1}^{N_x} \sum_{j=1}^{N_t} \left\| P_{u_j^0}\psi_i \right\|^2_{L^2(D)} \tag{49}$$

represents the mean squared sum of the norms of projections in the case of the empirical orthogonal modes (full Fourier modes) $\left\{\psi_i\right\}_{i=1}^{N_x}$ on the same data space, then

$$\left\| P_{V_0}\Phi \right\|^2_{L^2(D)} > \left\| P_{V_0}\Psi \right\|^2_{L^2(D)}. \tag{50}$$

This means that, for the purpose of digital twin modelling, the shape modes defined by Eq.(36) are qualitatively superior to the SVD empirical orthogonal modes.

We will demonstrate these consequences in the section dedicated to numerical results.

3.2 | Qualitative Analysis of the Digital Twin Data Model vs. Empirical Orthogonal Representation

A qualitative analysis of the orthogonality of the shape modes computed by the **ROD** algorithm introduced in this paper can be obtained from the Orthogonality Matrix (ORT). We define the ORT value for a pair of shape modes as

$$ORT_{ij} = \left\langle \phi_i(x), \phi_j(x) \right\rangle_{L^2(D)} = \int_D \phi_i(x)\,\phi_j(x)\,dx. \tag{51}$$

Normally, the computed ORT_{ij} takes values in the interval [0, 1], because the ROD leading shape modes are normalized vectors. In our case, we consider the shape modes to be orthogonal to each other if

$$ORT_{ij} = \begin{cases} 1, & i = j \\ 0, & i \neq j. \end{cases} \tag{52}$$

We introduce $\langle\cdot\rangle_T$ as a time average operator over $\left[t_1, T\right]$ corresponding to the arithmetic time-average of equally spaced elements of the interval $\left[t_1, T\right]$

$$\langle f(t)\rangle_T = \frac{1}{N_t} \sum_{i=1}^{N_t} f\left(t_i\right), \quad t_i \in \left\{t_1, t_2, ..., t_{N_t} = T\right\}. \tag{53}$$

The absolute error given by the **ROD** algorithm between the exact solution and the digital twin data model is defined by relation:

$$Error^{DTM} = \left\langle \left\| u(x,t) - u^{DTM}(x,t) \right\|_2 \right\rangle_T, \quad t \in \left[t_1, T\right]. \tag{54}$$

The correlation coefficient is used as additional metric to validate the quality of the digital twin data model over the exact solution and has the following expression:

$$Corr^{DTM} = \left\langle \frac{\left\| u(x,t)\, u^{DTM}(x,t) \right\|_2^{\,2}}{\left\| u(x,t)^2 \right\|_2 \left\| u^{DTM}(x,t)^2 \right\|_2} \right\rangle_T, \quad t \in \left[t_1, T\right]. \tag{55}$$

In the same manner, we define the absolute error between the exact solution and the Fourier representation having the following expression:

$$Error^{Fourier} = \left\langle \left\| u(x,t) - u^{Fourier}(x,t) \right\|_2 \right\rangle_T, \quad t \in \left[t_1, T\right], \tag{56}$$

4 | TIME SIMULATION OF THE DIGITAL TWIN DATA MODEL BY DEEP LEARNING

The randomized orthogonal decomposition **(ROD)** algorithm, previously described, allows the identification of the leading shape modes and their associated coefficients in discrete form. In the following, we aim to identification of a time simulated

digital twin data model of the form:

$$u^{DTM}(x,t) = \sum_{j=1}^{N_{DMD}} s_j(t)\,\phi_j(x), \quad t \in [0,T], \tag{57}$$

where ϕ_j, $j = 1, ..., N_{DMD}$ are the shape modes and $s_j(t)$, $j = 1, ..., N_{DMD}$ represent the continuous time simulated coefficients of the DTM.

Nonlinear AutoRegressive models with eXogenous inputs (NLARX) represent a novel approach in the field of nonlinear system identification by deep learning. Since the emergence of artificial neural networks as numerical tools, NLARX models have been used for various purposes, ranging from simulation[87], to nonlinear predictive control[88] or higher order nonlinear optimization problems[89].

In this paper we employ the application of NLARX for a high-fidelity time simulation of the coefficients of the digital twin data model (57).

Let $a(t)$ be the system input represented by the modal amplitudes calculated by randomized orthogonal decomposition at discrete time instances $t \in \left\{t_1, ..., t_{N_t}\right\}$ and $s(t)$ be the output.

The formulation of the NLARX model can be described as:

$$s(t) = f\left[s(t-1), ..., s\left(t-n_a\right), a\left(t-n_k\right), ..., a\left(t-n_k-n_b+1\right)\right] + e(t), \quad t \in [0,T], \tag{58}$$

where: n_a is the integer number of past output terms,

n_b is the number of past input terms used to predict the current output,

n_k is the pure input delay,

f is a nonlinear function implemented by an artificial neural network and

$e(t)$ represents the modeling error.

Each output of NLARX model (58) is a function of regressors that are transformations of past inputs and past outputs. Usually this function has a linear block and a nonlinear block. The model output is the sum of the outputs of the two blocks. The NLARX model training can be cast as a non-linear unconstrained optimization problem:

$$\theta\left(n_a, n_b, n_k\right) = \arg\min \frac{1}{2N_t} \sum_{i=1}^{N_t} \left\| s\left(t_i\right) - a\left(t_i\right) \right\|_2, \tag{59}$$

where the training set consists of the measured input $a(t)$, $s(t)$ is the continuous NLARX output, $\|\cdot\|_2$ is the L_2 norm and $\theta\left(n_a, n_b, n_k\right)$ represents the parameter vector of the nonlinear function f.

The NLARX structure can accommodate the dynamics of the system by feeding previous network outputs back into the input layer. It also enables the user to define how many previous output and input time steps are required for a best representation of the systems dynamics. One of most important task in application of NLARX network is a proper selection of inputs, input delays and output delays. The algorithm we have implemented automatically modifies the network parameters $\theta\left(n_a, n_b, n_k\right)$ over the complete trajectory to achieve the minimal value of (59).

We have implemented the nonlinear estimator f in the form of a cascade forward neural network with 10 hidden layer sizes. In the next section, we will detail the numerical results.

5 | NUMERICAL RESULTS

In the following we present numerical results demonstrating the computational performances of the Randomized Orthogonal Decomposition (**ROD**) introduced in this paper, associated with Deep Learning (DL) time simulation. We show that the output of this procedure is a high fidelity model of reduced complexity that has the main feature to mirror the original process behavior and has the capability to be real time simulated with highest precision, i.e. we produce a *Digital Twin Data Model (DTM)*.

The test problem used in this paper consists of the viscid Burgers equation model (1). Both the numerical accuracy and the computational efficiency of the DTMs are considered on the three experiments with three different initial conditions outlined in Section 2.1.

5.1 | The Exact Solutions

The computational domain considered is $[0, L]$, where $L = 2$, the computational time is $[0, T]$, where $T = 3$, viscosity parameter in the Burgers equation is $\nu = 10^{-2}$ for all three experiments. The computational domain is uniformly discretized by using $N = 100$ grid points, which yields a mesh-size $\Delta x = 0.02$.

Eq. (2), representing the initial condition in the case of Experiment 1, yields a sinusoidal pulse with abrupt change of slope at the extremities of the domain. The initial value problem with discontinuous initial condition of the form (3) is called a Riemann problem. This setting yields a shock wave phenomenon. We take the assumption $u_L = 0.1,\ u_R = 0.5$. In the case of Experiment 3, the initial condition (4) generates an even more complicated movement of the pulse. All three experiments yield phenomena that are challenging to capture with standard numerical schemes.

Using the Cole-Hopf transformation (6) we obtain the analytic solution to the Burgers problem (1) in the case of all three experiments, in the form (18), (19) and (20), respectively, as we detailed in Section 6. Next, we calculate numerically the exact solutions in the three test cases applying the technique of the Gauss-Hermite quadrature (13) with $n = 100$ nodes. (see Section 2.3).

Figure 2 illustrates the exact solutions for the three experiments considered.

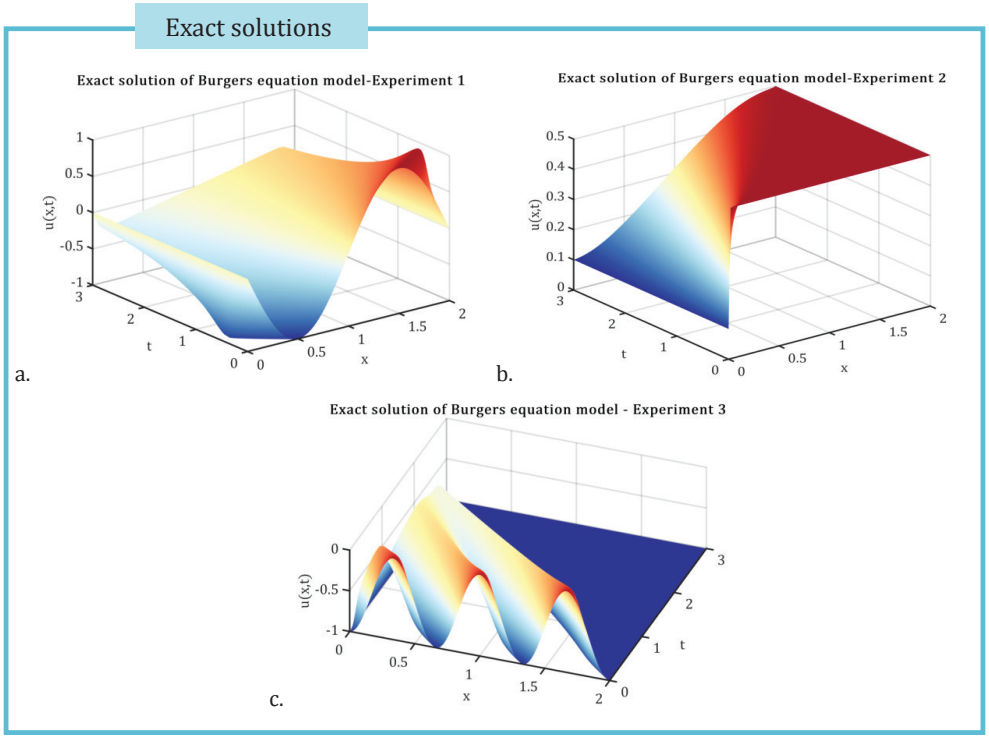

FIGURE 2 The exact solution of viscid Burgers equation model in the case of all three experiments, with initial conditions (2), (3), (4), respectively.

5.2 | The Digital Twin Data Models (DTMs) by Randomized Orthogonal Decomposition (ROD)

The Digital Twin Data Models of form (31) are created by the Randomized Orthogonal Decomposition Algorithm **(ROD)** as high fidelity surrogates for the three Burgers problems investigated here. For this scope, the training data comprises of

$N_t + 1 = 300 + 1$ total number of snapshots taken in time at regularly spaced time intervals $\Delta t = 0.01$,

$N_x = 101$ number of spatial measurements per time snapshot.

The Randomized Orthogonal Decomposition Algorithm presented in Section 3.1 finds the optimal dimension N_{DTM} of the space where the leading shape modes live, as the solution to the multiobjective optimization problem with nonlinear constraints

(32). The **ROD** algorithm solves this problem and finds Pareto front of the two fitness functions using a genetic algorithm. Figure 3 illustrates the objectives of the optimization problem (32) and the Pareto front solution, for the three experiments, respectively.

In the case of Experiment 1, the space dimension of the leading modes is $N_{DTM} = 10$. In the case of Experiment 2, the digital twin model for the Riemann problem dynamics has the space dimension of the leading modes $N_{DTM} = 20$. In the case of Experiment 3, the complexity of the pulse is mirrored by a digital twin model with a higher dimension, i.e. $N_{DTM} = 45$. In all three cases, the running CPU time of the **ROD** algorithm is extremely low, see Figure 4.

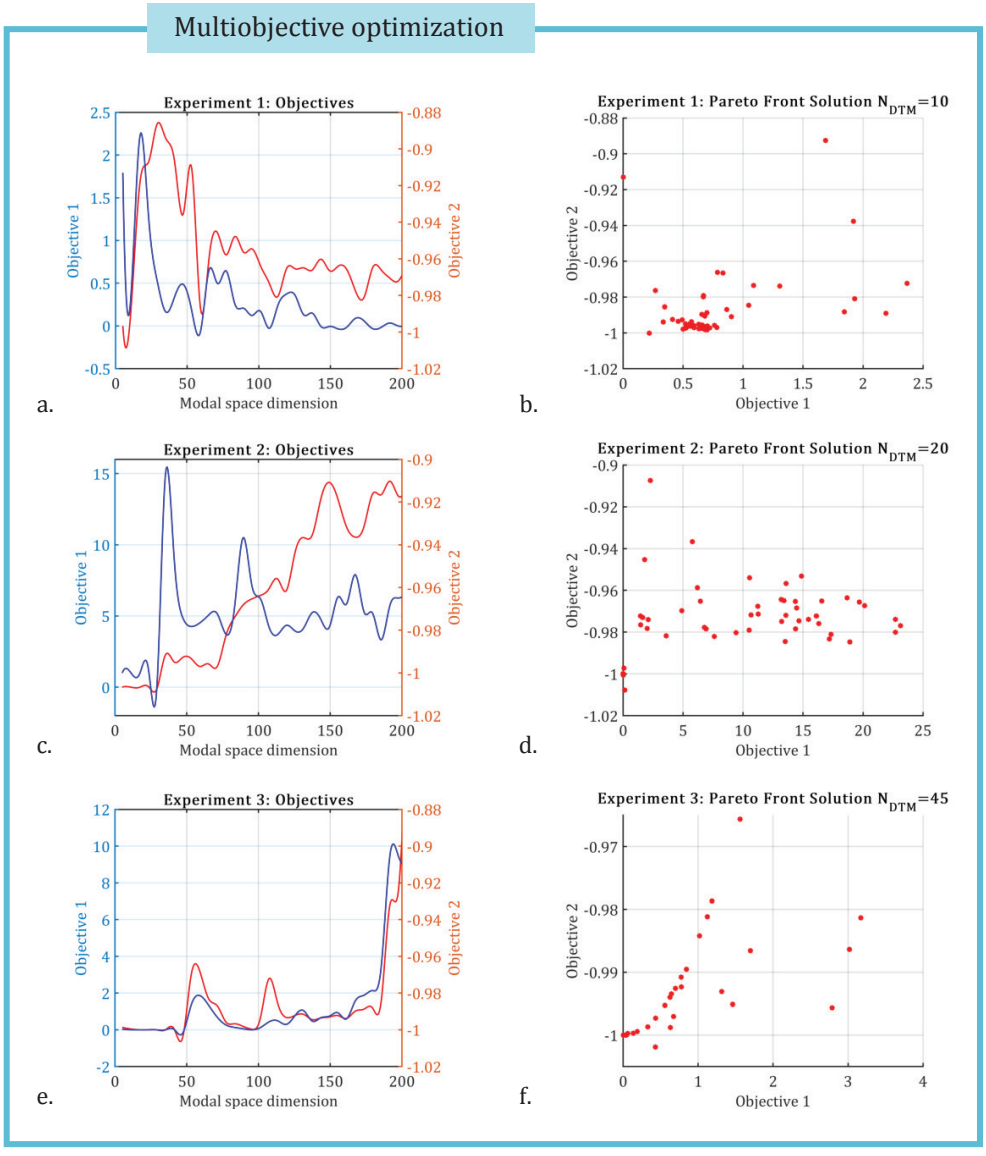

FIGURE 3 The objectives of the optimization problem (32) and the Pareto front solution obtained by genetic algorithm, for the three experiments, respectively.

The output of the Randomized Orthogonal Decomposition (**ROD**) algorithm introduced in this paper is illustrated in Figures 5-7. The digital twin data models are produced by **ROD** for the case of the three investigated experiments. The figures present also the leading shape modes and the corresponding growing amplitudes that contribute to the assembly of the DTMs.

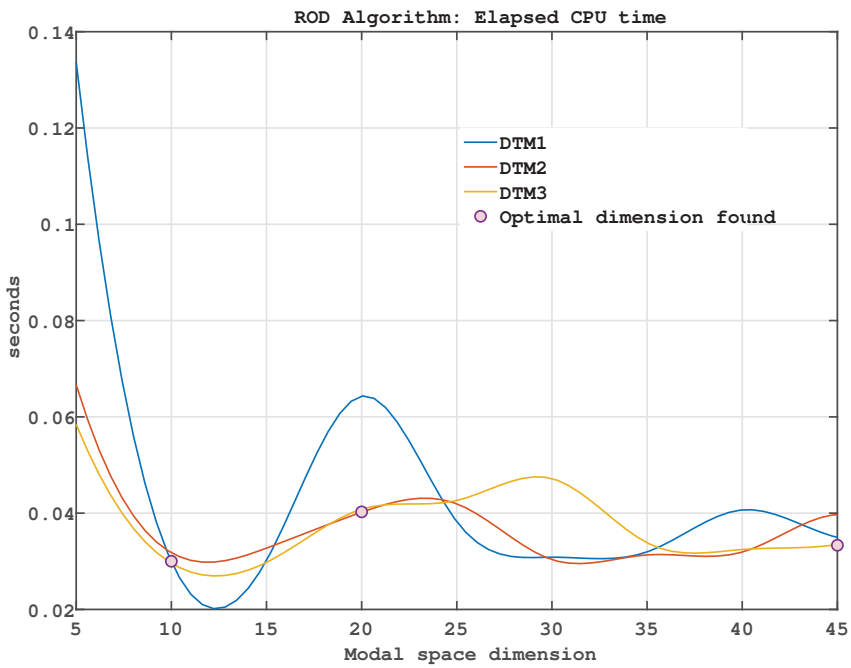

FIGURE 4 The running CPU time of the **ROD** algorithm, for the three experiments, respectively.

TABLE 1 Qualitative analysis of the DTMs.

Test case	DTM complexity[1]	DTM Absolute error[2]	DTM Correlation[3]
Experiment 1	$N_{DTM} = 10$	8.7264×10^{-7}	1.0000
Experiment 2	$N_{DTM} = 20$	6.4552×10^{-8}	1.0000
Experiment 3	$N_{DTM} = 45$	2.9684×10^{-7}	1.0000

[1]Leading shape modes space dimension.
[2]DTM Absolute error is given by Eq.(54).
[3]DTM Correlation is given by Eq.(55).

5.3 | Qualitative Analysis of the DTMs

The **ROD** algorithm determines the optimal shape vectors dimension and calculates also the leading shape modes and their corresponding growing amplitudes. Thus the Digital Twin Data Model (31) is created, having by definition the smallest error and the highest correlation in relation to the original data model.

In order to perform a qualitative analysis of the DTMs, we present in Table 1 the explicit results to the multiobjective optimization problem (32) solved by the **ROD** algorithm, i.e. the space dimension of the leading shape modes, the absolute error given by Eq.(54) and the correlation coefficient given by Eq.(55) between the exact solution and the digital twin model, in the case of the three investigated experiments.

Analysing the results presented in Table 1, it is obvious that the **ROD** algorithm creates models that are perfectly correlated with the original data (i.e. $Corr^{DTM} = 1$) for all three test cases, having absolute errors of order $Erorr^{DTM} < \mathcal{O}(10^{-7})$.

In order to compare the computational efficiency of the ROD modes with Fourier modes, we provide in Table 2 the qualitative error in reconstructed field using the SVD empirical orthogonal representation with the same complexity, respectively considering 10 modes with Experiment 1, 20 modes with Experiment 2 and 45 modes with Experiment 3.

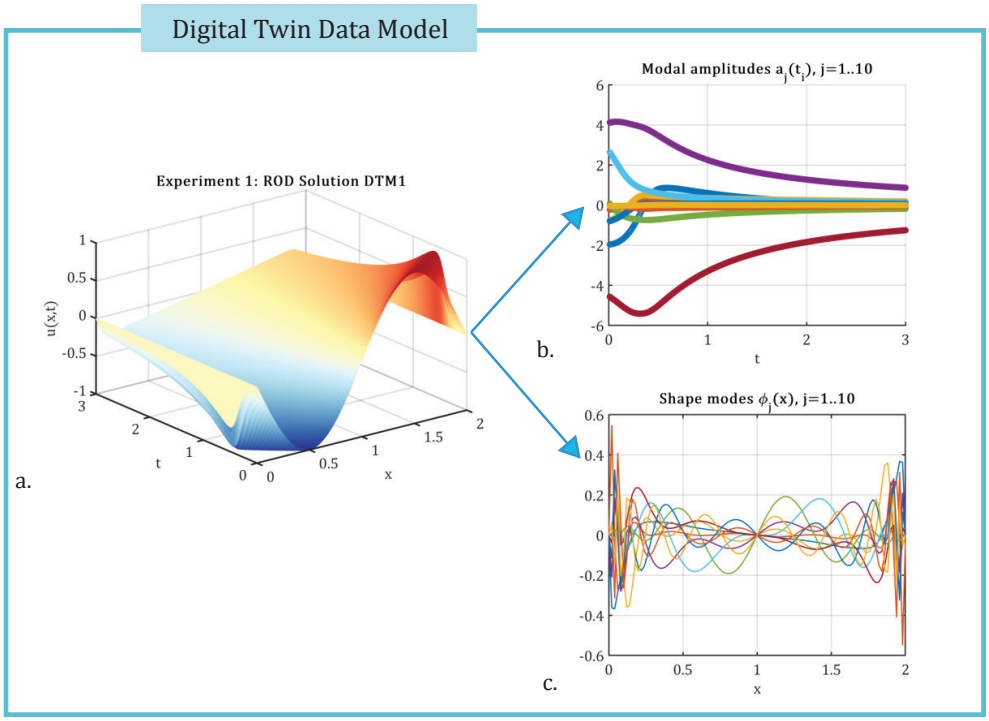

FIGURE 5 a.The digital twin model as the solution of ROD Algorithm of viscid Burgers equation model in the case of Experiment 1; b.The growing amplitudes; c.The corresponding leading shape modes.

TABLE 2 Qualitative analysis of the SVD empirical orthogonal representation.

Test case	**Model complexity**[1]	**Absolute error**[2]
Experiment 1	$N_x = 10$	5.4969×10^{-7}
Experiment 2	$N_x = 20$	3.4481×10^{-7}
Experiment 3	$N_x = 45$	3.9166×10^{-6}

[1]Fourier modes space dimension.
[2]Absolute error is given by Eq.(56).

We notice from Table 2 that the absolute error of Fourier series representation is with an order of magnitude greater than the DTM absolute error. This demonstrates that the ROD modes are comparable to SVD Fourier modes in term of computational efficiency. The most notable feature of SVD is that orders its basis from the highest to lowest contribution often referred as energy of the singular values. Thus, SVD Fourier decomposition provides a tailored orthonormal basis for a particular flow field by minimizing the L_2 norm between the original flow and the reconstructed flow.

The selection of modes based on their energy ranking is effective only in certain situations, as reported by many researchers [78,68]. There are also modes that apparently have a weak energy contribution but they exhibit rapid growth with lower amplitudes or they consist of high amplitudes fast damped modes, and therefore they may be representative in improving the flow digital twin data model. A major advantage of ROD over SVD Fourier representation consists in producing a significantly reduced size spectrum which incorporates the most influential shape modes. As a consequence, ROD algorithm omits a further selection criterion, that is most often a subjective one. We will demonstrate in the following that the ROD mods are qualitatively superior to the SVD Fourier modes.

For checking the orthogonality of the DTMs shape modes computed by the **ROD** algorithm, we compute the orthogonality matrix described in Section 3.2, for the case of the three experiments investigated here. The next figures present the ORT

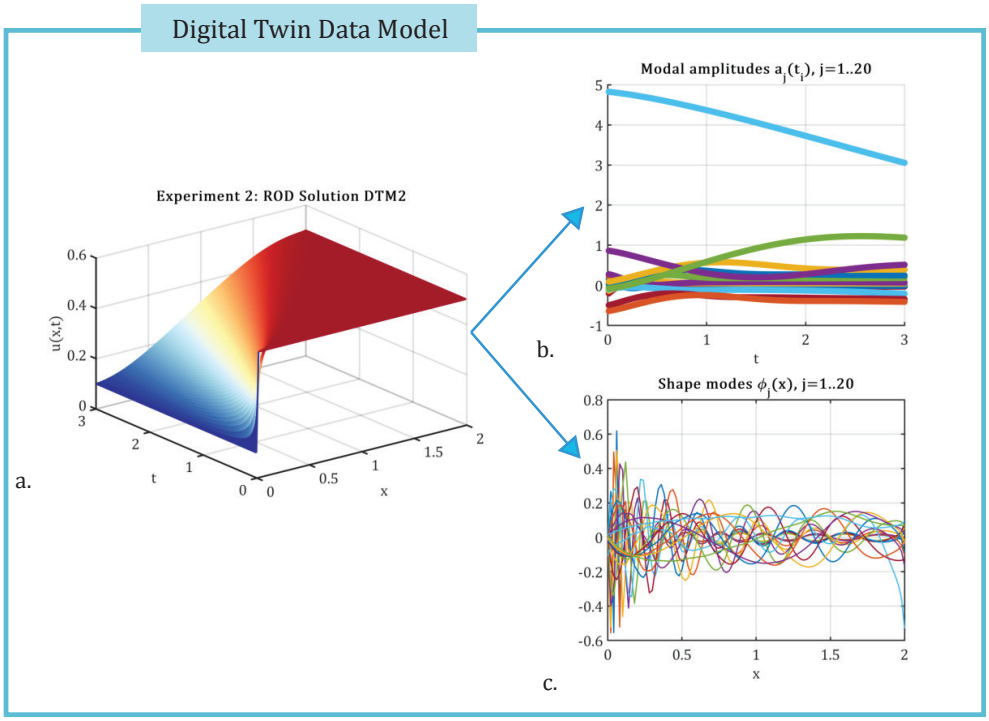

FIGURE 6 a.The digital twin model as the solution of ROD Algorithm of viscid Burgers equation model in the case of Experiment 2; b.The growing amplitudes; c.The corresponding leading shape modes.

TABLE 3 Qualitative analysis of the shape modes projection.

Test case	$\left\|P_{V_0}\Phi\right\|^2_{L^2(D)}$ †	$\left\|P_{V_0}\Psi\right\|^2_{L^2(D)}$ ‡	$\left\|P_{V_0}\Phi\right\|^2_{L^2(D)} / \left\|P_{V_0}\Psi\right\|^2_{L^2(D)}$
Experiment 1	56.6294	3.5029	16.1666
Experiment 2	25.7805	3.5427	7.2770
Experiment 3	25.2690	4.7435	5.3271

†ROD Shape Modes Projection Norm given by Eq.(48).
‡Full Fourier Modes Projection Norm given by Eq.(49).

values for each pair of leading shape modes, which we have previously defined in Eq.(51), where the zero value guarantees the orthogonality of the shape modes to each other.

Next, we show numerically that the leading shape modes Φ (36) computed by **ROD** algorithm maximize their projection on the data space, by comparison with the projection given by the full Fourier representation (28), i.e. we show that relation (50) is true.

Figure 9 illustrates the squared norms of the projections of the leading shape modes produced by ROD on the data space (left), vs. the squared norms of the modes projection in the case of the full Fourier representation, for the three investigated experiments (right).

Table 3 presents the mean squared sum of the projection norms and highlights that the ROD shape modes maximize their projection compared to the Fourier modes, in the case of all three experiments investigated in this paper, especially in the case of experiments 2 and 3 of high complexity.

Thus, we have demonstrated that the leading modes computed by Randomized Orthogonal Decomposition algorithm are qualitatively superior to the Fourier modes.

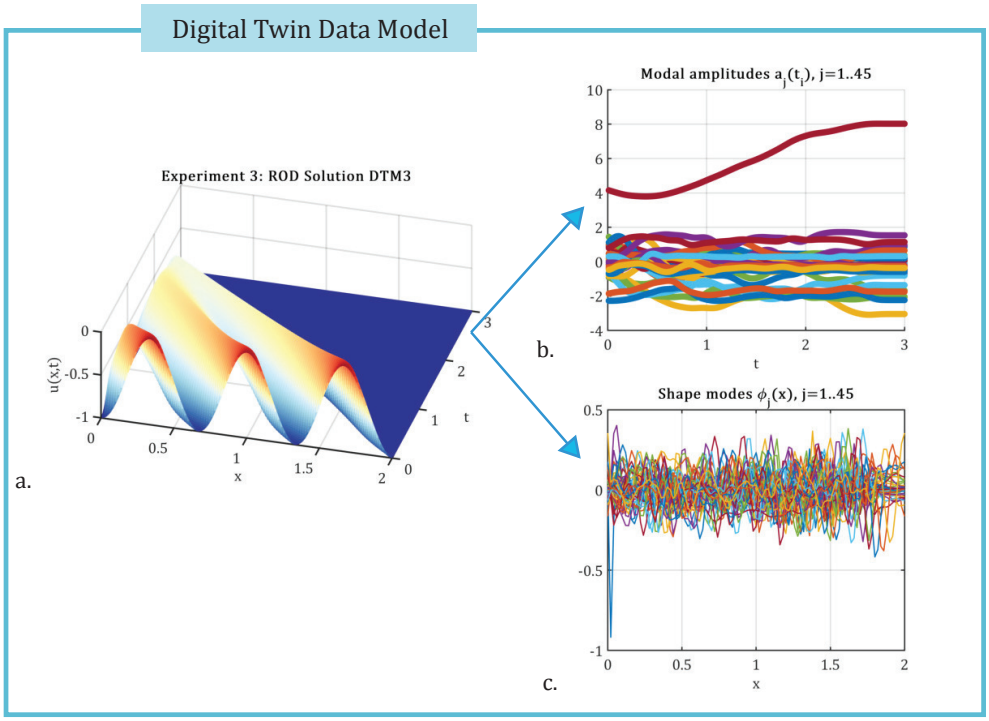

FIGURE 7 a.The digital twin model as the solution of ROD Algorithm of viscid Burgers equation model in the case of Experiment 3; b.The growing amplitudes; c.The corresponding leading shape modes.

5.4 | Time Simulation of the DTM Models

In this section we present the results of time simulated digital twin models of the form (57), using the technique of Deep Learning, which we have presented in Section 4.

The randomized orthogonal decomposition (ROD) algorithm previously described allows the identification of the leading shape modes and their associated coefficients in discrete form. Using Nonlinear AutoRegressive models with eXogenous inputs (NLARX) we perform a high-fidelity time simulation of the coefficients of the digital twin model in two steps.

1. **Step1: Optimal NLARX model.** First our algorithm identifies the optimal NLARX model of form (58), in the sense of Eq.(59), for each input amplitude $a\left(t_i\right)$, $t_i \in \left[t_1, T\right]$. We seek for NLARX models having up to two past output terms, having up to three past input terms used to predict the current output, the pure input delay is set not to exceed 5. We have implemented the nonlinear estimator f in form of a cascade forward neural network with 10 hidden layer sizes, see Figure 10.

2. **Step2: Time simulation of the optimal NLARX model.** In this second stage, we simulate the NLARX models constructed in the first stage and also we perform a two-fold Input-Output validation of the simulated response. This means that we use, one at a time, the first two thirds of the snapshots as training data, while the rest are used for validation of the simulated response. Then we reduce to the first third of the snapshots as training data, while the rest are used for validation of the simulated response.

Figures 11-13 illustrate the two-fold Input-Output validation for three randomly chosen temporal coefficients, as simulated responses of the optimal NLARX models, in the case of Experiment 1, 2 and 3, respectively. These figures highlight that the deep learning NLARX models simulate the responses with high accuracy, even when we reduce the dimension of the training data set at the first third of the data. Performance indicators for the deep learning procedure are also illustrated.

Next, we assembly the time simulated digital twin model in the form given by Eq.(57), for the three experiments investigated and we compare the output response with the exact solution in term of absolute local error, see Figure 14.

Figure 15 illustrates the running CPU time, for the phase of Deep Learning NLARX models simulations, with respect to the modal space dimension optimized in the case of the three experiments considered. The elapsed CPU time was recorded for two

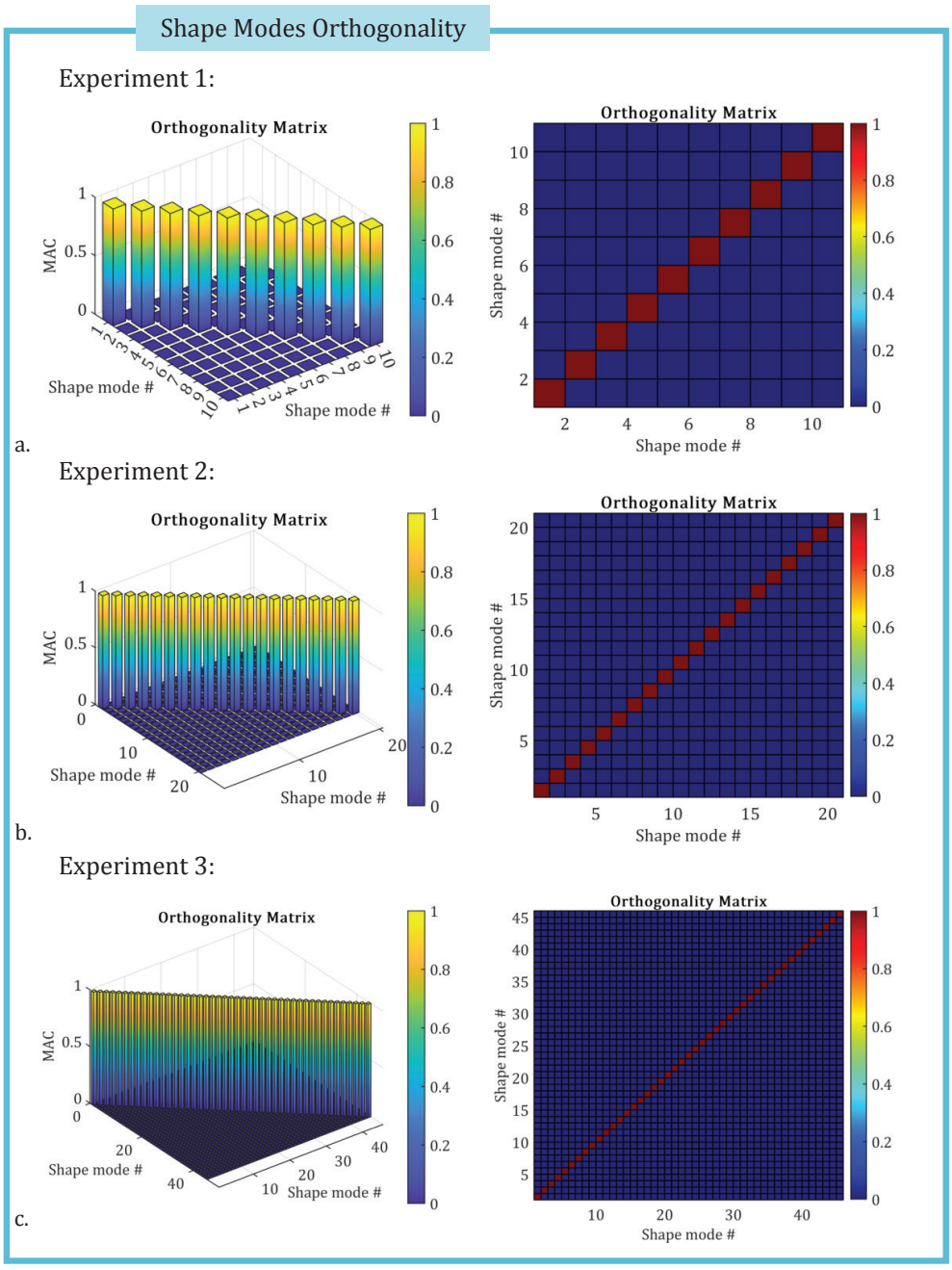

FIGURE 8 The orthogonality matrix, for the case of three investigated experiments, respectively. The ORT values given by Eq.(51) guarantee the orthogonality of the shape modes to each other.

consecutive computer runs. The computations and plots have been carried out using in-house scripts written in Matlab R2022a, on i7-7700K processor.

6 | CONCLUSIONS

The present investigation has focused on a subject of great interest in data science: we introduce a new framework to assembly *digital twin data models* of reduced complexity that mirror the dynamics of fluid flows with highest accuracy.

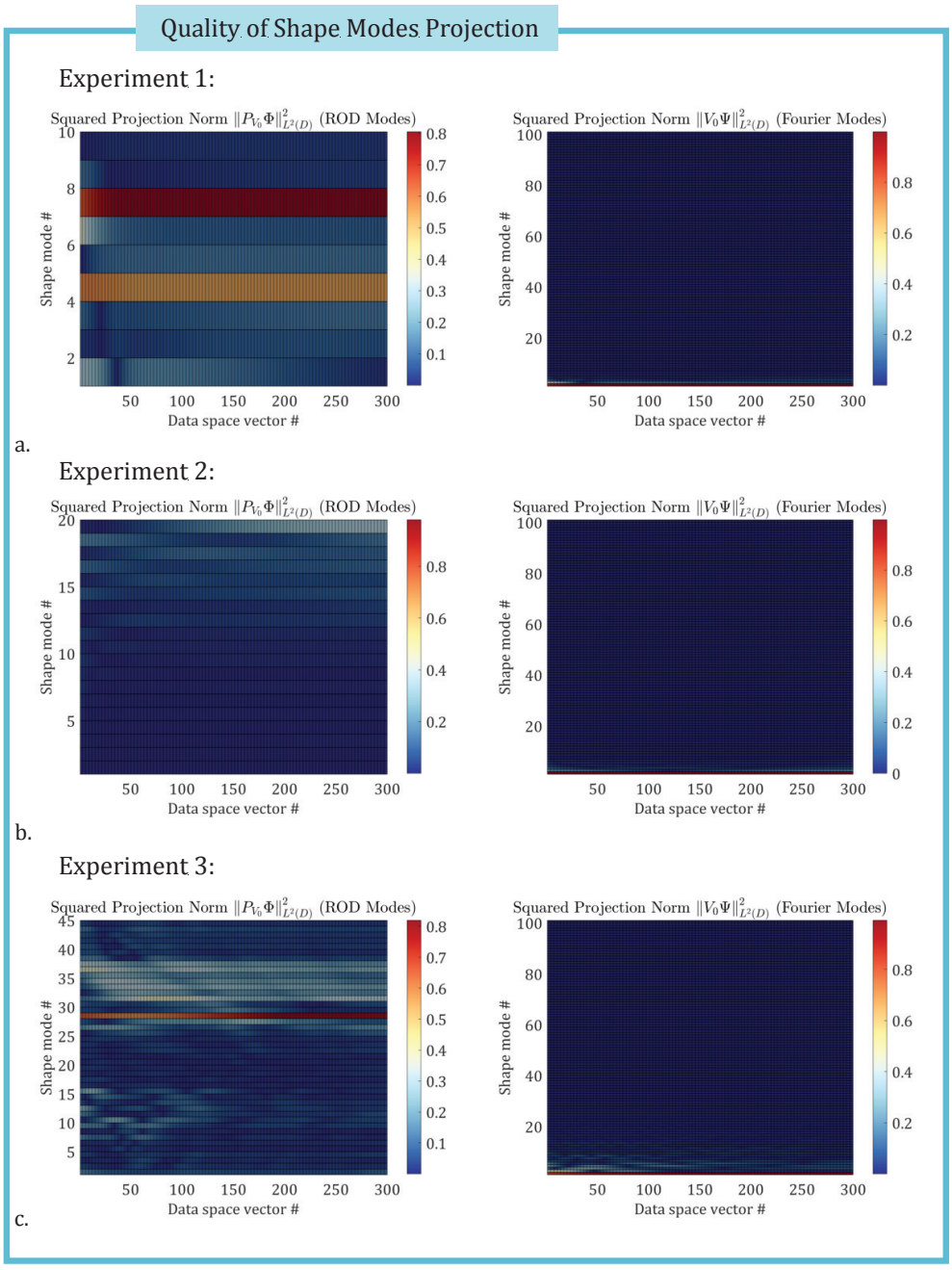

FIGURE 9 The squared norms of the projections of the leading shape modes produced by ROD on the data space (left), vs. the squared norms of the modes projection in the case of the full Fourier representation, for the three investigated experiments (right).

To the best of our knowledge, the present paper is the first work that introduces the algorithm of Randomized Orthogonal Decomposition (ROD) with application to fluid dynamics. The approach consists of two phases. First, we derived a new numerical algorithm to obtain a reduced order digital twin data model of the flow dynamics on the basis of Randomized Orthogonal Decomposition (**ROD**) of the data. In the second phase, we involve the state-of-the-art artificial intelligence Deep Learning (DL) to perform a real-time adaptive calibration of the digital twin model (DTM) and to obtain the time response of the DTM. Thus the digital twin data model is created, having by definition the smallest error and the highest correlation in relation to the original data.

We introduced several key innovations in the present approach.

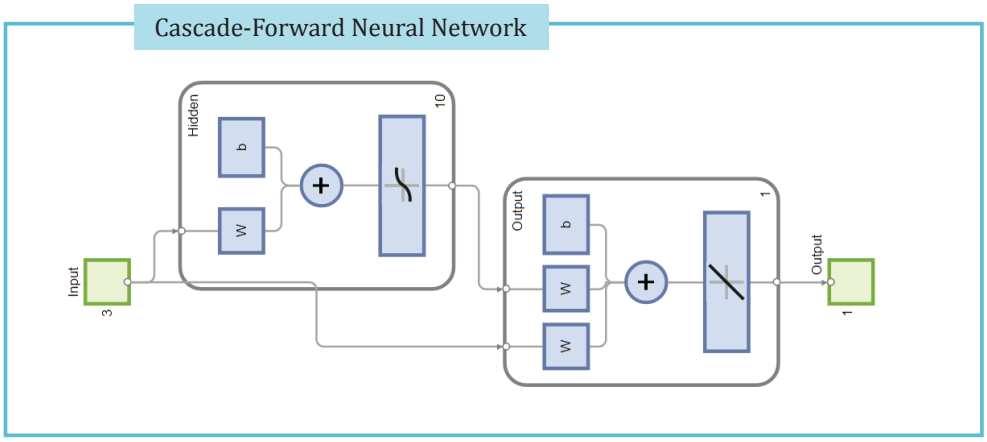

FIGURE 10 The cascade forward neural network with 10 hidden layer sizes, used as nonlinear estimator for the NLARX models.

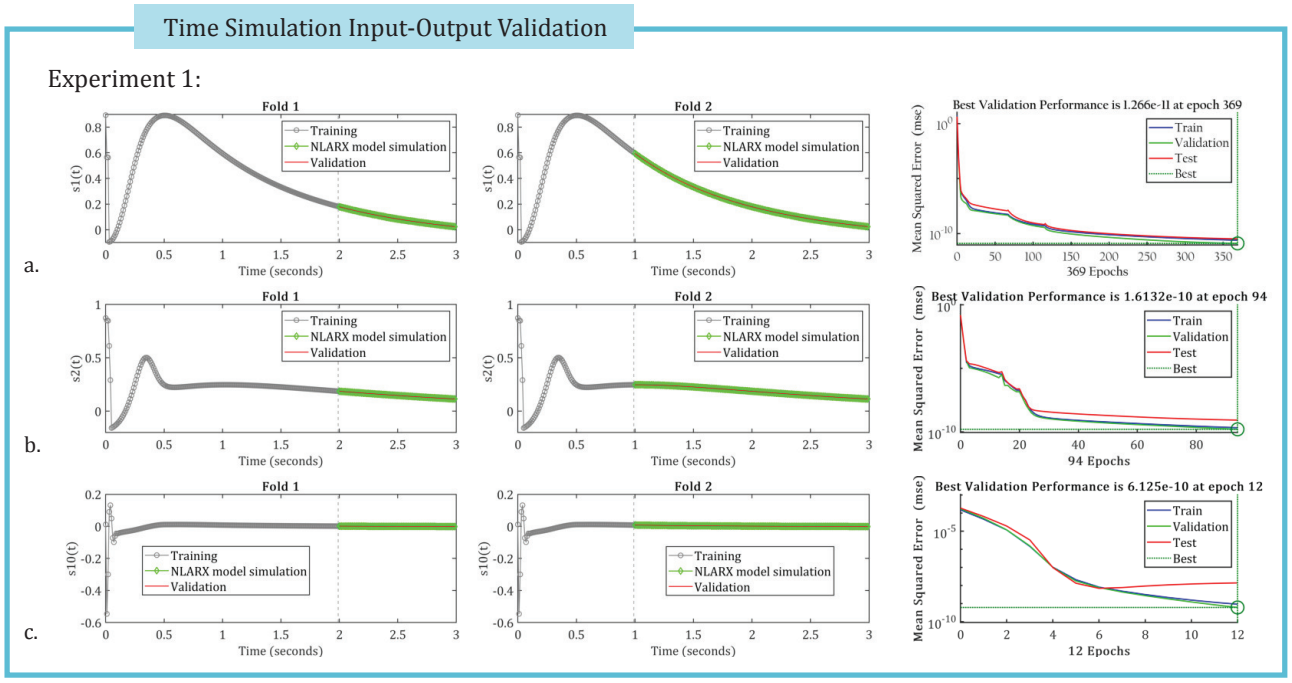

FIGURE 11 The two-fold Input-Output validation of the first two and the last temporal coefficients, as simulated responses of the optimal NLARX models, in the case of Experiment 1. Performance indicators for the deep learning procedure are illustrated.

We reduce the problem dimension by using a randomized singular value decomposition (RSVD) technique. Including data randomization has the major benefit of not requiring additional criteria to select the shape modes, as it is done in case of dynamic mode decomposition (DMD) or proper orthogonal decomposition (POD). Our algorithm that includes the RSVD finds the optimal reduced order subspace that contains the leading shape modes.

We have introduced in this paper a mathematical method to produce the shape modes that are orthonormal to each other.

We proved that the leading shape modes produced by Randomized Orthogonal Decomposition algorithm are qualitatively superior to the SVD empirical orthogonal modes, in the sense that the ROD modes maximize their projection on the data space, compared to the Fourier modes, in the case of all three experiments of high complexity investigated in this paper. Consequently, we proved that a much smaller number of terms is required in the construction of mathematical model.

We proved that randomized orthogonal decomposition outperformes SVD Fourier methods and mitigates the projection error formulating a multiobjective optimization problem.

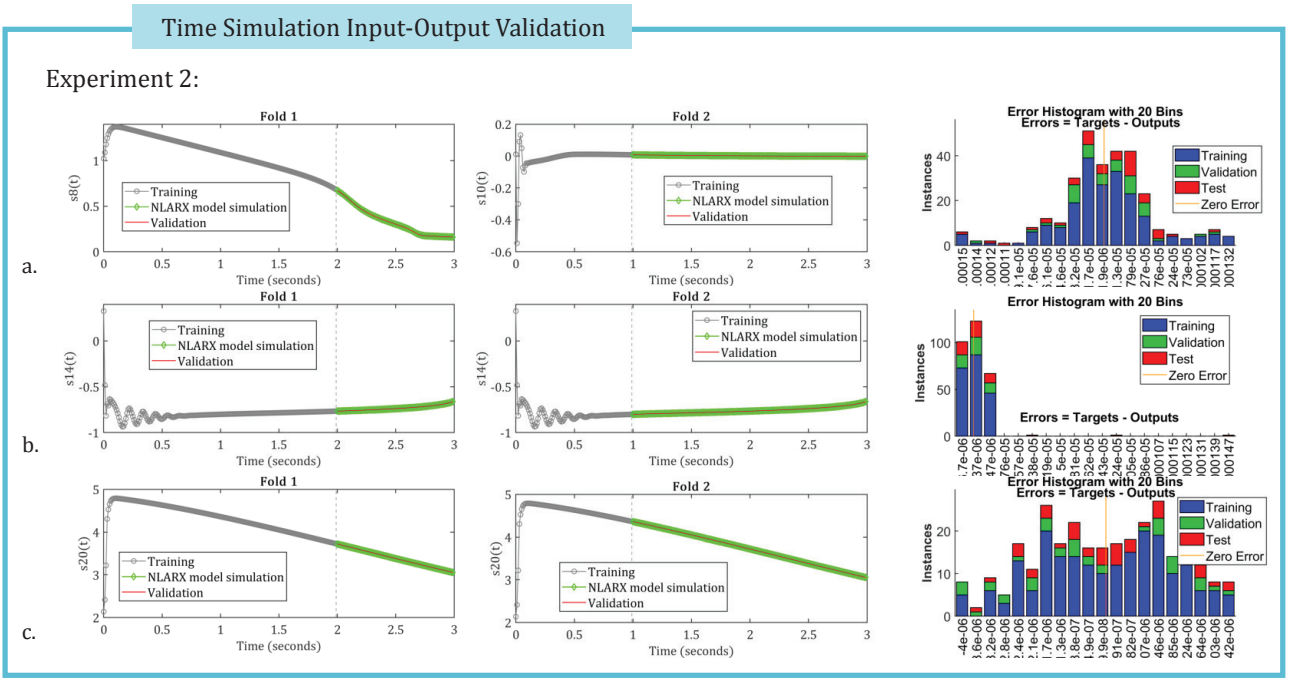

FIGURE 12 The two-fold Input-Output validation of three temporal coefficients, as simulated responses of the optimal NLARX models, in the case of Experiment 2. Performance indicators for the deep learning procedure are illustrated.

We proved that the digital twin data models are perfectly correlated with the original data and have the ability to be simulated in time with great precision. We performed the two-fold Input-Output validation and we highlighted that the deep learning models simulate the responses with high accuracy, even when we reduce the dimension of the training data set at the first third of the data.

The running CPU time, for the phase of Deep Learning NLARX models simulations, with respect to the modal space dimension is less than an hour, for the most complex experiment considered.

We conclude that Randomized Orthogonal Decomposition with Deep Learning technique can successfully bypass classic techniques like adjoint model reduction, POD-DEIM or Galerkin projection methods, that are much more computationally expensive and do not always have great precision. In a future paper we will consider testing the proposed method on two-dimensional datasets with applications originating from different fields.

Author contributions

Diana A. Bistrian: Conceptualization (lead); Methodology (lead); Writing – review and editing (equal). **Omer San:** Conceptualization (equal); Methodology (equal); Writing – review and editing (equal). **Ionel M. Navon:** Conceptualization (equal); Methodology (equal); Review (equal).

Conflict of interest

The authors declare no potential conflict of interests.

References

1. Holmes P, Lumley J, Berkooz G. *Turbulence, coherent structures, dynamical systems and symmetry*. Cambridge Univ. Press . 1996.

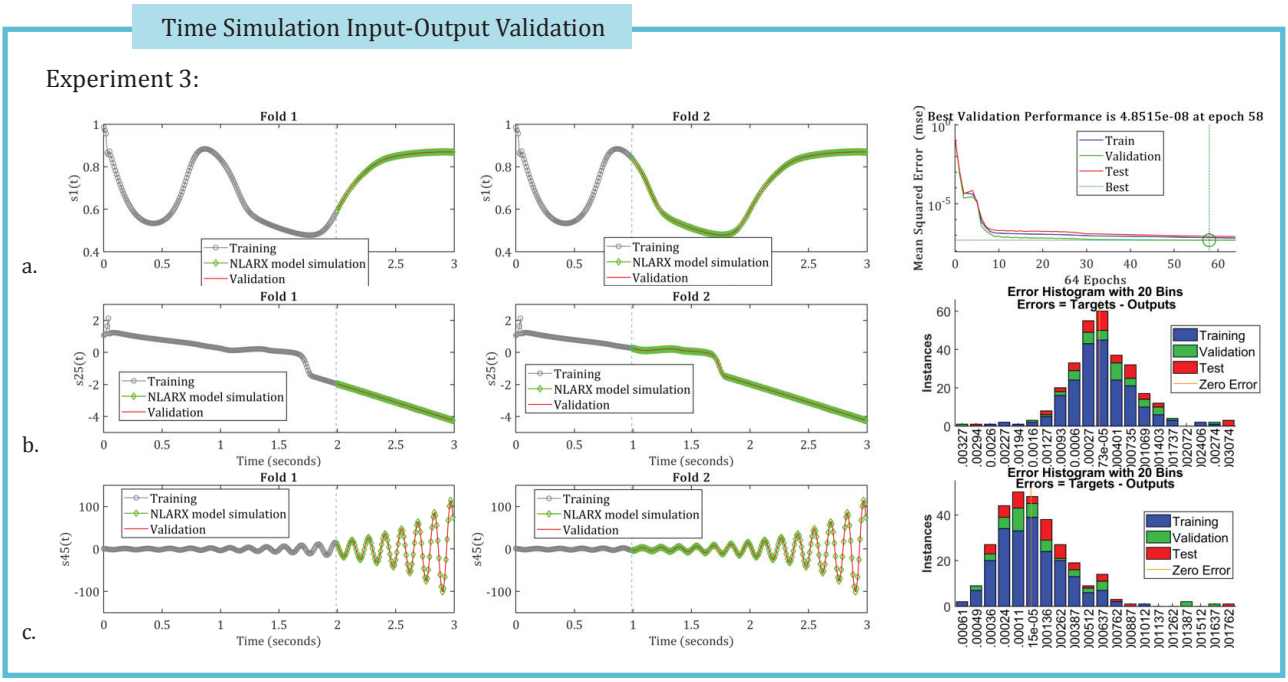

FIGURE 13 The two-fold Input-Output validation of three temporal coefficients, as simulated responses of the optimal NLARX models, in the case of Experiment 3. Performance indicators for the deep learning procedure are illustrated.

2. Rasheed A, San O, Kvamsdal T. Digital Twin: Values, Challenges and Enablers From a Modeling Perspective. *IEEE Access* 2020; 8: 21980 - 22012. doi: 10.1109/ACCESS.2020.2970143

3. Wang Z, Akhtar I, Borggaard J, Iliescu T. Proper orthogonal decomposition closure models for turbulent flows: A numerical comparison. *Computer Methods in Applied Mechanics and Engineering* 2012; 10(26): 237–240.

4. Xiao D, Heaney CE, Fang F, et al. A domain decomposition non-intrusive reduced order model for turbulent flows. *Computers and Fluids* 2019; 182: 15–27.

5. Gunzburger M, Iliescu T, Mohebujjaman M, Schneier M. Nonintrusive stabilization of reduced order models for uncertainty quantification of time-dependent convection-dominated flows. *Preprint arXiv* 2018; 1810.08746.

6. Luchtenburg DM, Rowley CW. Model reduction using snapshot-based realizations. In: American Physical Society; 2011: H19.004.

7. Liberge E, Hamdouni A. Reduced order modelling method via proper orthogonal decomposition (POD) for flow around an oscillating cylinder. *Journal of Fluids and Structures* 2010; 26: 292311.

8. Xiao D, Fang F, Heaney CE, Navon IM, Pain CC. A domain decomposition method for the non-intrusive reduced order modelling of fluid flow. *Computer Methods in Applied Mechanics and Engineering* 2019; 354: 307–330.

9. San O, Staples A, Wang Z, Iliescu T. Approximate deconvolution large eddy simulation of a barotropic ocean circulation model. *Ocean Modelling* 2011; 40(2): 120-132.

10. San O, Iliescu T. A stabilized proper orthogonal decomposition reduced-order model for large scale quasigeostrophic ocean circulation. *Advances in Computational Mathematics* 2014; 41(5): 12891319.

11. Dumon A, Allery C, Ammar A. Proper Generalized Decomposition method for incompressible Navier-Stokes equations with a spectral discretization. *Applied Mathematics and Computation* 2013; 219(15): 8145-8162.

12. Osth J, Noack BR, Krajnovic S, Barros D, Boree J. On the need for a nonlinear subscale turbulence term in POD models as exemplified for a high-Reynolds-number flow over an Ahmed body. *Journal of Fluid Mechanics* 2014; 747: 518-544.

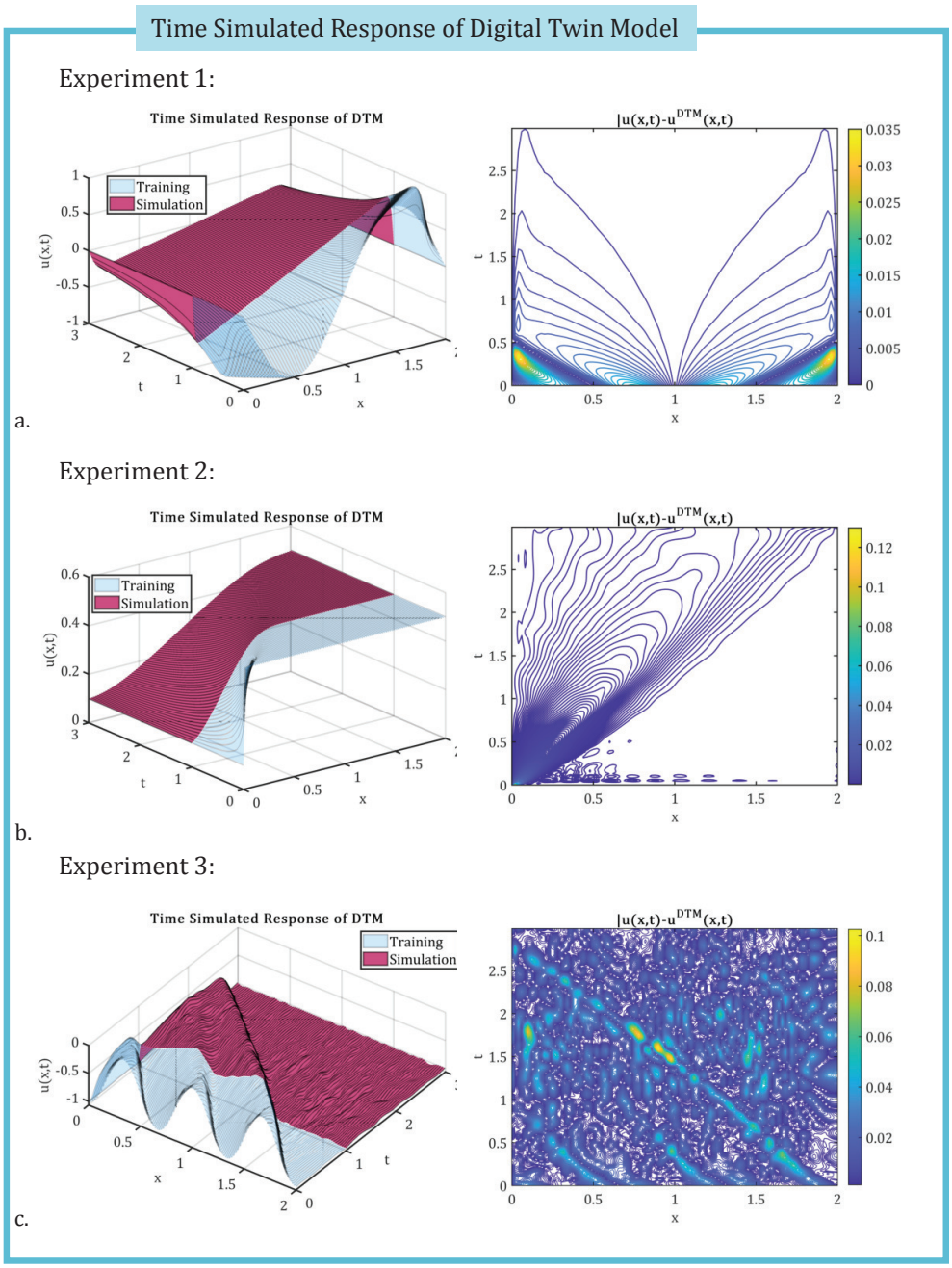

FIGURE 14 Time response of digital twin models, in the case of all three experiments vs. local error between original data and simulated DTM response.

13. Buljak V, Maier G. Proper Orthogonal Decomposition and Radial Basis Functions in material characterization based on instrumented indentation. *Engineering Structures* 2011; 33: 492501.

14. Brunton S, Kutz J. *Data-driven science and engineering: Machine learning, dynamical systems and control*. Cambridge University Press . 2022.

15. Xiao M, Breitkopf P, Coelho RF, Knopf-Lenoir C, Villon P, Zhang W. Constrained Proper Orthogonal Decomposition based on QR-factorization for aerodynamical shape optimization. *Applied Mathematics and Computation* 2013; 223: 254-263.

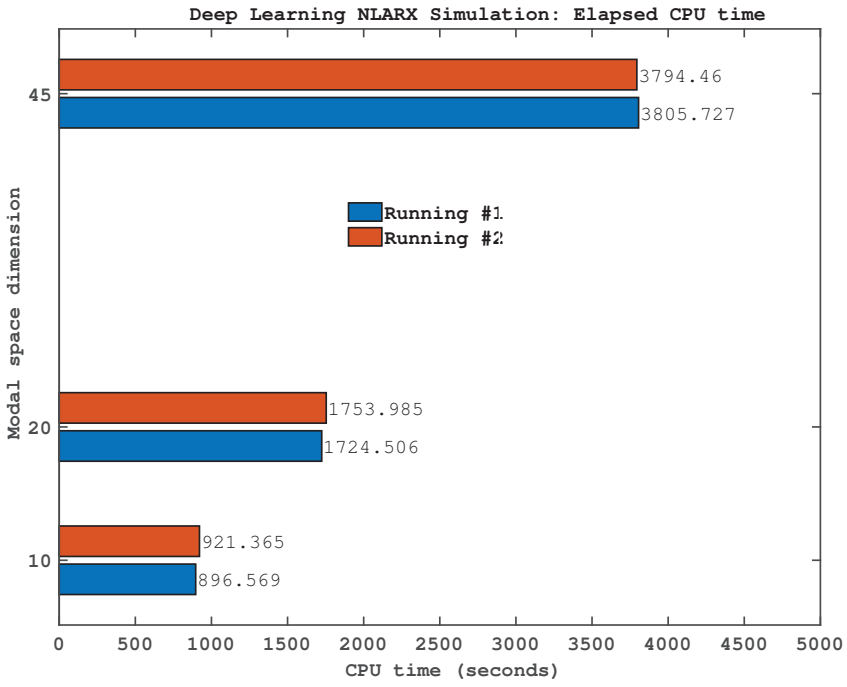

FIGURE 15 The running CPU time, for the phase of Deep Learning NLARX models simulations, with respect to the modal space dimension optimized in the case of the three experiments considered.

16. Li S, Kaiser E, Laima S, Li H, Brunton S, Kutz J. Discovering time-varying aerodynamics of a prototype bridge by sparse identification of nonlinear dynamical systems. *Physical Review E* 2019; 100(2).

17. Kaiser E, Kutz J, Brunton S. Sparse identification of nonlinear dynamics for model predictive control in the low-data limit. In: . 474. ; 2018: 20180335.

18. Wang Y, Ding X, Hu K, Fang F, Navon I, Lin G. Feasibility of DEIM for retrieving the initial field via dimensionality reduction. *Journal of Computational Physics* 2021; 429: 110005.

19. Stefanescu R, Hite J, Cook J, Smith R, Mattingly J. Surrogate-based robust design for a non-smooth radiation source detection problem. *Algorithms* 2019; 12(6): 113.

20. Dimitriu G, Stefanescu R, Navon IM. POD-DEIM approach on dimension reduction of a multi-species host-parasitoid system. *Ann. Acad. Rom., Sci. Ser. Math. Appl.* 2015; 7(1): 173-188.

21. Winton C, Pettway J, Kelley CT, Howington S, Eslinger OJ. Application of Proper Orthogonal Decomposition (POD) to inverse problems in saturated groundwater flow. *Advances in Water Resources* 2011; 34: 1519-1526.

22. Chen WS. Use of recurrence plot and recurrence quantification analysis in Taiwan unemployment rate time series. *Physica A: Statistical Mechanics and its Applications* 2011; 390(7): 1332–1342.

23. Chen KK, Tu JH, Rowley CW. Variants of dynamic mode decomposition: boundary condition, Koopman and Fourier analyses. *Nonlinear Science* 2012; 22: 887-915.

24. Cao Y, Zhu J, Luo Z, Navon IM. Reduced order modeling of the upper tropical Pacific ocean model using proper orthogonal decomposition.. *Computers and Mathematics with Applications* 2006; 52(8-9): 1373-1386.

25. Cao Y, Zhu J, Navon I, Luo Z. A reduced order approach to four-dimensional variational data assimilation using proper orthogonal decomposition. *International Journal for Numerical Methods in Fluids* 2007; 53(10): 1571-1583.

26. Xiao D, Du J, Fang F, Pain C, Li J. Parameterised non-intrusive reduced order methods for ensemble Kalman filter data assimilation. *Computers & Fluids* 2018; 177(69-77).

27. Sierra C, Metzler H, Muller M, Kaiser E. Closed-loop and congestion control of the global carbon-climate system. *Climatic Change* 2021; 165(1): 1-24.

28. Dawson S, Brunton S. Improved approximations to Wagner function using sparse identification of nonlinear dynamics. *AIAA Journal* 2022; 60(3): 1691-1707.

29. Xiao D, Heaney CE, Mottet L, et al. A reduced order model for turbulent flows in the urban environment using machine learning. *Building and Environment* 2019; 148: 323-337. doi: 10.1016/j.buildenv.2018.10.035

30. San O, Maulik R, Ahmed M. An artificial neural network framework for reduced order modeling of transient flows. *Communications in Nonlinear Science and Numerical Simulation* 2019; 77: 271-287. doi: 10.1016/j.cnsns.2019.04.025

31. Kaptanoglu A, Callaham J, Hansen C, Brunton S. Machine Learning to Discover Interpretable Models in Fluids and Plasmas. *Bulletin of the American Physical Society* 2022.

32. Owens K, Kutz J. Data-driven discovery of governing equations for coarse-grained heterogeneous network dynamics. *arXiv preprint* 2022(arXiv:2205.10965).

33. Cheng M, Fang F, Pain C, Navon I. Data-driven modelling of nonlinear spatio-temporal fluid flows using a deep convolutional generative adversarial network. *Computer Methods in Applied Mechanics and Engineering* 2020; 365: 113000.

34. Bistrian DA, Navon IM. An improved algorithm for the shallow water equations model reduction: Dynamic Mode Decomposition vs POD. *International Journal for Numerical Methods in Fluids* 2015; 78(9): 552-580.

35. Champion KP, Brunton SL, Kutz JN. Discovery of nonlinear multiscale systems: Sampling strategies and embeddings. *SIAM Journal on Applied Dynamical Systems* 2019; 18(1): 312-333.

36. Amsallem D, Farhat C. Stabilization of projection-based reduced-order models. *International Journal for Numerical Methods in Engineering* 2011; 91(4): 358-377.

37. Iliescu T. ROM Closures and Stabilizations for Under-Resolved Turbulent Flows. In: ; 2022.

38. Mauroy A, Sootla A, Mezic I. *The Koopman Operator in Systems and Control: Theory, Numerics, and Applications*. Springer . 2019.

39. Ahmed SE, San O, Bistrian DA, Navon IM. Sampling and resolution characteristics in reduced order models of shallow water equations: Intrusive vs nonintrusive. *International Journal for Numerical Methods in Fluids* 2020; 92(8): 992–1036.

40. Koopman B. Hamiltonian systems and transformations in Hilbert space. *Proc. Nat. Acad. Sci.* 1931; 17: 315-318.

41. Mezic I. Spectral properties of dynamical systems, model reduction and decompositions. *Nonlinear Dynamics* 2005; 41(1-3): 309-325.

42. Mezic I. Koopman operator, geometry, and learning. *arXiv preprint* 2020; arXiv:2010.05377.

43. Rowley CW, Mezic I, Bagheri S, Schlatter P, Henningson DS. Reduced-order models for flow control: balanced models and Koopman modes. In: . 18. Seventh IUTAM Symposium on Laminar-Turbulent Transition, IUTAM Bookseries; 2010: 43-50.

44. Chen KK, Tu JH, Rowley CW. Variants of dynamic mode decomposition: boundary condition, Koopman and Fourier analyses. *Nonlinear Science* 2012; 22: 887-915.

45. Mezic I. Koopman Operator, Geometry, and Learning of Dynamical Systems. *Notices of the American Mathematical Society* 2021; 68(7): 1087-1105.

46. Li B, Ma Y, Kutz J, Yang X. The Adaptive Spectral Koopman Method for Dynamical Systems. *arXiv preprint* 2022; arXiv:2202.09501.

47. Schmid PJ, Sesterhenn J. Dynamic mode decomposition of numerical and experimental data. In: . 53(15). American Physical Society. ; 2008; San Antonio, Texas.

48. Rowley CW, Mezic I, Bagheri S, Schlatter P, Henningson DS. Spectral analysis of nonlinear flows. *Journal of Fluid Mechanics* 2009; 641: 115-127.

49. Schmid P. Dynamic mode decomposition of numerical and experimental data. *Journal of Fluid Mechanics* 2010; 656: 5-28.

50. Mezic I. On Numerical Approximations of the Koopman Operator. *Mathematics* 2022; 10: 1180.

51. Frederich O, Luchtenburg DM. Modal analysis of complex turbulent flow. In: ; 2011; Ottawa, Canada,.

52. Schmid PJ, Violato D, Scarano F. *Decomposition of time-resolved tomographic PIV*. Springer-Verlag . 2012.

53. Alla A, Kutz JN. Nonlinear model order reduction via dynamic mode decomposition. *SIAM Journal on Scientific Computing* 2017; 39(5): B778–B796.

54. Kaheman K, Brunton S, Kutz J. Automatic differentiation to simultaneously identify nonlinear dynamics and extract noise probability distributions from data. *Machine Learning: Science and Technology* 2022; 3(1): 015031.

55. Sahba S, Sashidhar D, Wilcox C, McDaniel A, Brunton S, Kutz J. Dynamic mode decomposition for aero-optic wavefront characterization. *Optical Engineering* 2022; 61(1): 013105.

56. Brunton SL, Brunton BW, Proctor JL, Kutz JN. Koopman Invariant Subspaces and Finite Linear Representations of Nonlinear Dynamical Systems for Control. *PLoS ONE* 2016; 11(2): e0150171. doi: 10.1371/journal.pone.0150171

57. Kutz J, Sashidhar D, Sahba S, Brunton S, McDaniel A, Wilcox C. Physics-informed machine-learning for modeling aero-optics. *International Conference On Applied Optical Metrology* 2021; IV(11817): 70-77.

58. Percic M, Zelenika S, Mezic I. Artificial intelligence-based predictive model of nanoscale friction using experimental data. *Friction* 2021; 9(6): 1726-1748.

59. Pant P, Doshi R, Bahl P, Farimani AB. Deep learning for reduced order modelling and efficient temporal evolution of fluid simulations. *Physics of Fluids* 2021; 33: 107101.

60. Bistrian DA, Dimitriu G, Navon IM. Modeling dynamic patterns from COVID-19 data using randomized dynamic mode decomposition in predictive mode and ARIMA. In: . 2302. AIP Conference Proceedings; 2020: 080002.

61. Bistrian DA, Dimitriu G, Navon IM. Processing epidemiological data using dynamic mode decomposition method. In: . 2164. AIP Conference Proceedings; 2019: 080002.

62. Zheng J, Fang XWF, Li J, et al. Numerical study of COVID-19 spatial-temporal spreading in London. *Physics of Fluids* 2021; 33(4): 046605.

63. Kim S, Kim M, Lee S, Lee Y. Discovering spatiotemporal patterns of COVID-19 pandemic in South Korea. *Scientific Reports* 2021; 11: 24470.

64. Tu JH, Rowley CW, Luchtenburg DM, Brunton SL, Kutz JN. On dynamic mode decomposition: Theory and applications.. *Journal of Computational Dynamics* 2014; 1(2): 391–421.

65. Jovanovic MR, Schmid PJ, Nichols JW. Sparsity-promoting dynamic mode decomposition. *Physics of Fluids* 2014; 26: 024103.

66. Kutz JN, Fu X, Brunton SL. Multiresolution dynamic mode decomposition. *SIAM Journal on Applied Dynamical Systems* 2016; 15(2): 713–735.

67. Williams MO, Kevrekidis IG, Rowley CW. A datadriven approximation of the Koopman operator: extending Dynamic Mode Decomposition. *Nonlinear Science* 2015; 25: 1307–1346. doi: 10.1007/s00332-015-9258-5

68. Noack BR, Stankiewicz W, Morzynski M, Schmid P. Recursive dynamic mode decomposition of transient and post-transient wake flows. *Journal of Fluid Mechanics* 2016; 809: 843–872.

69. Proctor JL, Brunton SL, Kutz JN. Dynamic mode decomposition with control. *SIAM Journal of Applied Dynamical Systems* 2016; 15(1): 142–161.

70. Erichson NB, Donovan C. Randomized low-rank Dynamic Mode Decomposition for motion detection. *Computer Vision and Image Understanding* 2016; 146: 40–50.

71. Erichson NB, Brunton SL, Kutz JN. Compressed dynamic mode decomposition for background modeling. *Journal of Real-Time Image Processing* 2019; 16(5): 1479-1492.

72. Bistrian DA, Navon IM. Randomized dynamic mode decomposition for nonintrusive reduced order modelling. *International Journal for Numerical Methods in Engineering* 2017; 112: 3–25.

73. Ahmed SE, Dabaghian PH, San O, Bistrian DA, Navon IM. Dynamic mode decomposition with core sketch. *Physics of Fluids* 2022; 34: 066603.

74. Goldschmidt A, Kaiser E, Dubois J, Brunton S, Kutz J. Bilinear dynamic mode decomposition for quantum control. *New Journal of Physics* 2021; 23(3): 033035.

75. Le Clainche S, Vega JM. Higher Order Dynamic Mode Decomposition. *SIAM Journal on Applied Dynamical Systems* 2017; 16(2): 882-925. doi: 10.1137/15M1054924

76. Dimitriu G, Ştefănescu R, Navon IM. Comparative numerical analysis using reduced-order modeling strategies for nonlinear large-scale systems. *Journal of Computational and Applied Mathematics* 2017; 310: 32-43.

77. Bistrian DA, Susan-Resiga RF. Weighted proper orthogonal decomposition of the swirling flow exiting the hydraulic turbine runner. *Applied Mathematical Modelling* 2016; 40: 4057-4078.

78. Noack BR, Morzynski M, Tadmor G. *Reduced-Order Modelling for Flow Control*. Springer . 2011.

79. Tissot G, Cordier L, Benard N, Noack BR. Model reduction using Dynamic Mode Decomposition. *Comptes Rendus Mecanique* 2014; 342: 410-416.

80. Navon IM. A Numerov-Galerkin technique applied to a finite-ement shallow water equations model with enforced conservation of integral invariants and selective lumping. *Journal of Computational Physics* 1983; 52: 313-339.

81. Alekseev AK, Bistrian DA, Bondarev AE, Navon IM. On linear and nonlinear aspects of dynamic mode decomposition. *International Journal for Numerical Methods in Fluids* 2016; 82: 348–371. doi: 10.1002/fld.4221

82. Bistrian DA, Navon IM. The method of dynamic mode decomposition in shallow water and a swirling flow problem. *International Journal for Numerical Methods in Fluids* 2017; 83: 73–89.

83. Bistrian DA, Navon IM. Efficiency of randomised dynamic mode decomposition for reduced order modelling. *International Journal Of Computational Fluid Dynamics* 2018; 32(2-3): 88–103.

84. Brass H, Petras K. *Quadrature Theory. The Theory of Numerical Integration on a Compact Interval* . 2011.

85. Bai Z, Erichson NB, Meena MG, Taira K, Brunton SL. Randomized methods to characterize large-scale vortical flow networks. *PLoS ONE* 2019; 14(11): e0225265.

86. Erichson NB, Manohar K, Brunton SL, Kutz JN. Randomized CP tensor decomposition. *Machine Learning: Science and Technology* 2020; 1(2): 025012.

87. Nelles O. *Nonlinear System Identification: From Classical Approaches to Neural Networks and Fuzzy Models*. Springer . 2001.

88. Liu G, Kadirkamanathan V, Billings S. Predictive control for non-linear systems using neural networks. *International Journal of Control* 1998; 71: 1119-1132.

89. Peng H, Ozaki T, Haggan-Ozaki V, Toyoda Y. Structured parameter optimization method for the radial basis function-based state-dependent autoregressive model. *International Journal of Systems Science* 2002; 33: 1087-1098.

How to cite this article: Bistrian D.A., O. San, and I.M. Navon (2022), Digital Twin Data Modelling by Randomized Orthogonal Decomposition and Deep Learning, *International Journal for Numerical Methods in Engineering*, *2022;00:1–28*.